3. Antigenic peptides with non-natural replacements within the GH loop of FMDV

3.0 Introduction

In an attempt to analyse the contribution of each amino acid residue to the antigenicity of site A of FMDV C-S8c1, M. L. Valero and co-workers evaluated a set of 250 peptides corresponding to the systematic replacement of all residues within the sequence of peptide A15[1-3]. Peptide antigenicity was quantitated by competition ELISA, using a panel of seven anti-site A mAbs: SD6, 4C4, 5A2, 6D11, 7DJ1, 7FC12 and 7CA11. In this systematic screening, five singly replaced peptides were found to be antigenic for at least three mAbs, being comparable to or even better than the native A15 sequence. These peptides corresponded to the substitutions Thr137→Ile, Ala138→Phe, Ala140→Pro, Gly142→Ser and Thr148→Ile. Although the first two and the last residue replacements correspond to hyper-variable regions of the GH loop, the contrast in size between the Phe and the Ala residues, the structural "personality" of Pro and, even more, the Gly→Ser mutation within the highly conserved RGD motif, altogether raise many questions about what would be the contribution of these residues in antibody recognition.

In the present chapter, further studies on the above mentioned amino acid replacements are presented. Both the one-point mutants (Table 3.1), and a set of peptides reproducing all possible combinations of the five mutations were synthesised and antigenically characterised by SPR. Some NMR and X-ray diffraction studies were also performed, as a structural complement to the functional SPR characterisation of the peptide antigens.

3.1 Peptides that combine antigenicity-enhancing replacements in the GH loop

Thirty-one peptides, corresponding to the combinations of the five mutations (Table 3.1), were synthesised (Fig. 3.1, Table 3.2) by methods similar to those mentioned in chapter 2 and further described in section 4.2 (Materials & Methods).

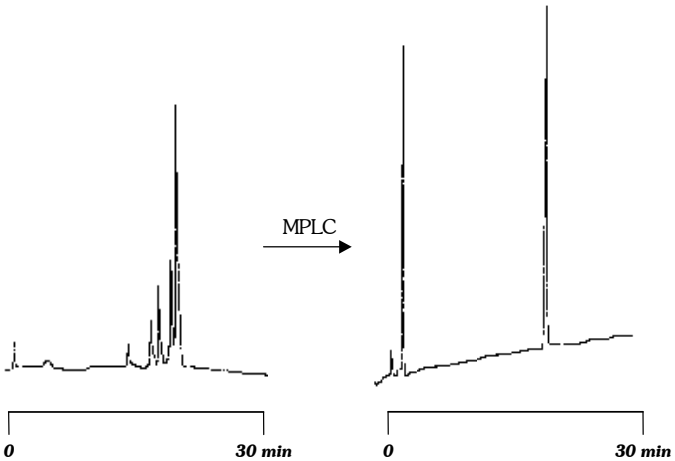

Figure 3. 1 HPLC of crude (left) and purified (right) peptide A15(138F,140P,142S), representative of the thirty-one 15-mers of this chapter.

Table 3.1 Pentadecapeptide library reproducing all possible combinations of the substitutions Thr137→Ile, Ala138→Phe, Ala140→Pro, Gly142→Ser and Thr148→Ile.

Name	***Sequence***	***Mutants***
A15	YTASARGDLAHLTTT	***GH loop of FMDV C-S8c1***
A15(137I)	-I----------	
A15(138F)	--F---------	
A15(140P)	----P-------	One-point
A15(142S)	------S-----	
A15(148I)	----------I-	
A15(137I,138F)	-IF---------	
A15(137I,140P)	-I--P-------	
A15(137I,142S)	-I----S-----	
A15(137I,148I)	-I---------I-	
A15(138F,140P)	--F-P-------	Two
A15(138F,142S)	--F---S-----	Point
A15(138F,148I)	--F--------I-	
A15(140P,142S)	----P-S-----	
A15(140P,148I)	----P------I-	
A15(142S,148I)	------S-----I-	
A15(137I,138F,140P)	-IF-P-------	
A15(137I,138F,142S)	-IF---S-----	
A15(137I,138F,148I)	-IF--------I-	
A15(137I,140P,142S)	-I--P-S-----	
A15(137I,140P,148I)	-I--P------I-	Three
A15(137I,142S,148I)	-I----S-----I-	Point
A15(138F,140P,142S)	--F-P-S-----	
A15(138F,140P,148I)	--F-P------I-	
A15(138F,142S,148I)	--F---S-----I-	
A15(140P,142S,148I)	----P-S-----I-	
A15(137I,138F,140P,142S)	-IF-P-S-----	
A15(137I,138F,140P,148I)	-IF-P------I-	
A15(137I,138F,142S,148I)	-IF---S-----I-	Four-point
A15(137I,140P,142S,148I)	-I--P-S-----I-	“
A15(138F,140P,142S,148I)	--F-P-S-----I-	“
A15(137I,138F,140P,142S,148I)	-IF-P-S-----I-	Five-point

Table 3.2 General data (yield and product characterisation by HPLC, ES or MALDI-TOF MS and AAA) of the syntheses of the 15-mer peptides.

Peptide	***Global yield (%)***	***Purity (% HPLC)***	***MW found***	***MW expected***	***AAA***
A15(137I)	89	99	1589.2	1589	Asp, 1.07 (1); Ser, 1.04 (1); Gly, 1.08 (1); Ala, 3.10 (3); Leu, 1.96 (2); His, 0.92 (1)
A15(138F)	65	97	1653.3	1653	Asp, 0.96 (1); Ser, 0.96 (1); Gly, 1.03 (1); Ala, 2.05 (2); Leu, 2.05 (2); His, 0.99 (1)
A15(140P)	84	98	1603.1	1603	Asp, 1.04 (1); Ser, 0.97 (1); Gly, 1.05 (1); Ala, 2.07 (2); Leu, 1.96 (2); Arg, 1.01 (1)
A15(142S)	79	99	1607.2	1607	Asp, 1.05 (1); Ser, 1.99 (2); Ala, 3.08 (3); Leu, 2.00 (2); His, 0.92 (1); Arg, 0.95 (1)
A15(148I)	87	98	1589.1	1589	Asp, 1.05 (1); Ser, 1.01 (1); Gly, 1.04 (1); Ala, 3.03 (3); Leu, 1.82 (2); Arg, 0.94 (1)
A15(IF)*	15	93	1665.1	1665	Asp, 1.00 (1); Ser, 0.98 (1); Gly, 1.03 (1); Ala, 1.98 (2); Leu, 1.98 (2); His, 1.02 (1)
A15(IP)	55	91	1615.6	1615	Asp, 1.06 (1); Ser, 1.00 (1); Gly, 1.10 (1); Ala, 1.93 (2); Pro, 0.99 (1); Arg, 1.02 (1)
A15(IS)	79	90	1619.2	1619	Asp, 0.99 (1); Ser, 2.07 (2); Ala, 3.08 (3); Leu, 2.03 (2); His, 0.88 (1); Arg, 0.95 (1)
A15(II)	78	97	1601.3	1601	Asp, 1.00 (1); Ser, 0.99 (1); Gly, 1.01 (1); Ala, 3.04 (3); His, 0.92 (1); Arg, 0.99 (1)
A15(FP)	72	95	1679.6	1679	Asp, 1.06 (1); Pro, 1.01 (1); Gly, 1.09 (1); Ala, 1.05 (1); Leu, 1.89 (2); Arg, 1.07 (1)
A15(FS)	86	89	1684.1	1684	Asp, 1.05 (1); Ser, 2.10 (2); Ala, 2.05 (2); Leu, 1.88 (2); His, 0.92 (1); Arg, 1.00 (1)
A15(FI)	86	91	1665.4	1665	Asp, 1.03 (1); Ser, 0.95 (1); Gly, 1.03 (1); Ala, 2.00 (2); His, 0.90 (1); Arg, 1.09 (1)
A15(PS)	81	87	1632.4	1633	Asp, 1.02 (1); Pro, 1.03 (1); Ala, 2.04 (2); Leu, 1.93 (2); His, 0.92 (1); Arg, 1.11 (1)
A15(PI)	79	89	1615.6	1615	Asp, 1.03 (1); Ser, 0.95 (1); Gly, 1.00 (1); Ala, 2.01 (2); His, 0.95 (1); Arg, 1.07 (1)
A15(SI)	79	86	1619.6	1619	Asp, 1.05 (1); Ser, 1.96 (2); Ala, 3.10 (3); Tyr, 0.87 (1); His, 0.92 (1); Arg, 1.14 (1)
A15(IFP)	78	94	1691.6	1691	Asp, 1.03 (1); Ser, 0.96 (1); Gly, 1.05 (1); Ala, 1.01 (1); Pro, 0.98 (1); Arg, 1.05 (1)
A15(IFS)	95	86	1694.5	1695	Asp, 1.10 (1); Ser, 1.90 (2); Tyr, 0.91 (1); Phe, 1.01 (1); His, 0.97 (1); Arg, 1.08 (1)
A15(IFI)	83	95	1677.4	1677	Asp, 1.01 (1); Ser, 0.91 (1); Gly, 1.01 (1); Ala, 1.97 (2); His, 1.07 (1); Arg, 1.04 (1)
A15(IPS)	82	94	1644.3	1645	Asp, 1.03 (1); Pro, 1.04 (1); Ala, 2.01 (2); Leu, 1.90 (2); His, 0.91 (1); Arg, 1.12 (1)
A15(IPI)	71	92	1626.6	1627	Asp, 1.05 (1); Ser, 0.99 (1); Pro, 1.00 (1); Gly, 1.08 (1); Ala, 1.93 (2); Arg, 1.03 (1)
A15(ISI)	80	92	1631.1	1631	Asp, 1.05 (1); Ser, 2.07 (2); Ala, 2.97 (3); Leu, 1.84 (2); His, 0.96 (1); Arg, 0.95 (1)
A15(FPS)	73	97	1708.3	1709	Asp, 0.97 (1); Ser, 1.97 (2); Ala, 1.04 (1); Leu, 2.08 (2); Phe, 1.03 (1); Arg, 1.02 (1)
A15(FPI)	87	90	1690.1	1691	Asp, 1.02 (1); Pro, 1.00 (1); Gly, 1.06 (1); Ala, 1.02 (1); Phe, 0.86 (1); His, 0.90 (1)
A15(FSI)	88	91	1695.0	1695	Asp, 1.07 (1); Ala, 2.09 (2); Leu, 1.85 (2); Tyr, 0.87 (1); Phe, 0.91 (1); His, 1.07 (1)
A15(PSI)	89	92	1645.0	1645	Asp, 1.00 (1); Pro, 1.02 (1); Ala, 2.02 (2); Tyr, 0.93 (1); His, 0.91 (1); Arg, 1.11 (1)
A15(IFPS)	77	95	1720.9	1721	Asp, 0.98 (1); Ser, 1.91 (2); Pro, 0.98 (1); Ala, 0.99 (1); His, 1.07 (1); Arg, 1.07 (1)
A15(IFPI)	74	94	1703.1	1703	Asp, 0.99 (1); Ser, 0.94 (1); Pro, 0.96 (1); Gly, 1.03 (1); Ala, 0.96 (1); Arg, 1.01 (1)
A15(IFSI)	84	98	1706.7	1707	Asp, 1.07 (1); Ser, 2.06 (2); Ala, 2.04 (2); Leu, 1.91 (2); His, 0.93 (1); Arg, 0.89 (1)
A15(IPSI)	80	91	1656.0	1657	Asp, 1.02 (1); Ser, 1.91 (2); Pro, 1.02 (1); Ala, 1.98 (2); His, 0.96 (1); Arg, 1.11 (1)
A15(FPSI)	56	92	1721.2	1721	Asp, 1.04 (1); Ser, 2.01 (2); Pro, 1.04 (1); Ala, 1.01 (1); Phe, 0.91 (1); Arg, 1.08 (1)
A15(IFPSI)	80	94	1732.1	1733	Asp, 1.09 (1); Ser, 2.03 (2); Pro, 1.02 (1); Ala, 1.05 (1); Leu, 1.99 (2); Arg, 0.95 (1)

Note: relative amino acid proportions given by AAA are followed by the expected value in parenthesis (for simplicity, mutant peptides are designed only with the capital case letter code for the replaced amino acids without the corresponding position number).* synthesis performed under sub-optimal conditions due to instrumental malfunction.

3.2 Analysis of the mutated peptides by direct kinetic SPR

Kinetic SPR screening of the thirty-one peptide antigens was performed as previously described in chapters 1 and 2. In this particular case, it was observed that most interactions could not be quantitated, either due to high association rates, extremely slow dissociation rates or even insufficient surface regeneration (Fig. 3.2). This was particularly frequent with mAbs 4C4 and 3E5. Also, surface saturation was observed for peptide concentrations higher than *ca.* 600 nM.

Interaction data that could be reasonably fitted as a 1:1 bimolecular interaction (Table 3.3) presented, in most cases, rate constants in the limit of reliable kinetic information[4-6]. Non-ideal effects, such as ligand rebinding in the dissociation phase, seemed to be affecting binding kinetics (Fig. 3.3).

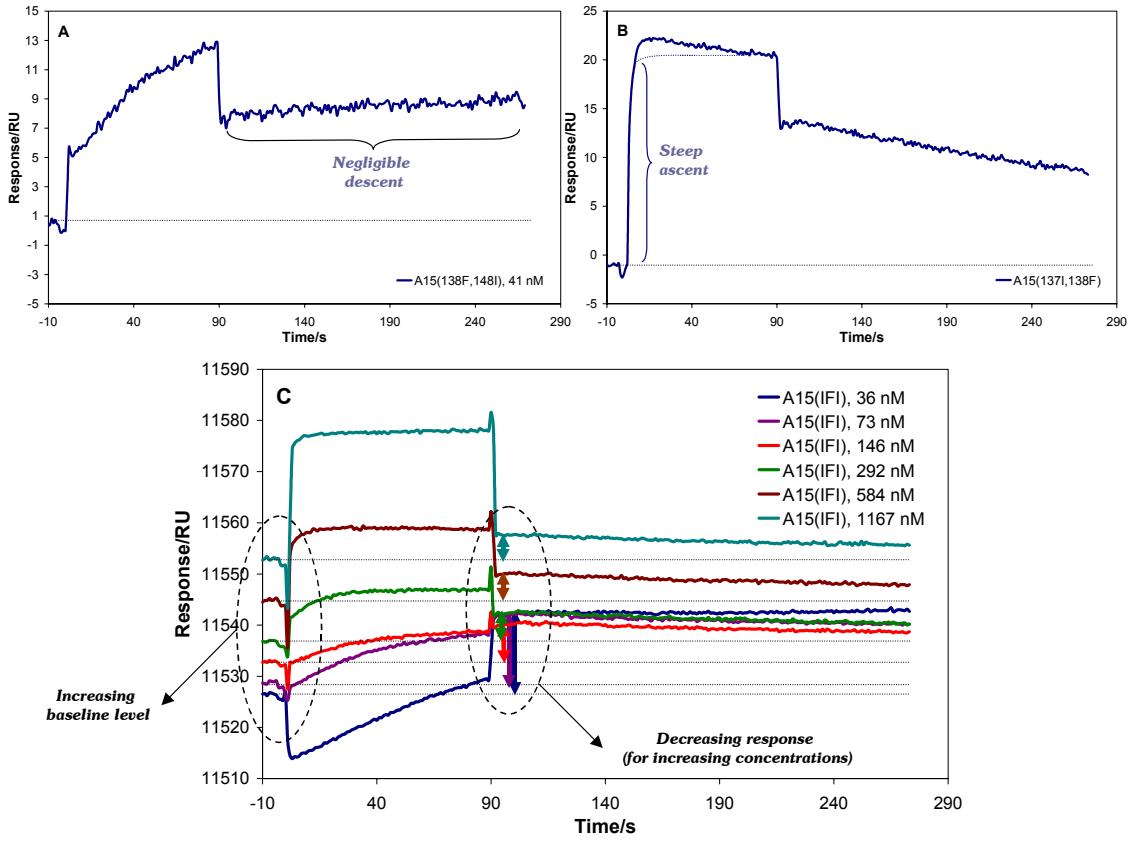

Figure 3. 2 Sensorgrams illustrating problems often observed in the kinetic SPR analysis of the interactions between anti-site A mAbs and peptides combining mutations Thr137→Ile, Ala138→Phe, Ala140→Pro, Gly142→Ser and Thr148→Ile; ***A***. extremely slow dissociation (as can be observed, slope is, in fact, positive, possibly due to the sum of a negligible dissociation slope and a positive slope from instrumental drift); ***B***. extremely fast association (a steep ascent can be observed, giving the sensorgram a square wave-like shape in the association phase); ***C***. Insufficient surface regeneration: the baseline level increases and the response level decreases from cycle to cycle.

mAb / Peptide	SD6			4C4			3E5		
	$k_a/M^{-1}s^{-1}$	k_d/s^{-1}	K_A/M^{-1}	$k_a/M^{-1}s^{-1}$	k_d/s^{-1}	K_A/M^{-1}	$k_a/M^{-1}s^{-1}$	k_d/s^{-1}	K_A/M^{-1}
A15	7.3×10^{4}	1.4×10^{-3}	$\mathbf{5.4\times10^{7}}$	3.8×10^{5}	1.9×10^{-3}	$\mathbf{1.9\times10^{8}}$	1.6×10^{5}	1.6×10^{-3}	$\mathbf{9.4\times10^{7}}$
A15(137I)	9.6×10^{4}	5.0×10^{-4}	$\mathbf{1.9\times10^{8}}$	2.9×10^{5}	2.0×10^{-3}	$\mathbf{1.4\times10^{8}}$	3.5×10^{5}	1.0×10^{-3}	$\mathbf{3.4\times10^{8}}$
A15(138F)	8.6×10^{4}	3.9×10^{-3}	$\mathbf{2.2\times10^{7}}$	5.5×10^{5}	5.7×10^{-3}	$\mathbf{9.8\times10^{7}}$	6.0×10^{5}	1.4×10^{-3}	$\mathbf{4.0\times10^{8}}$
A15(140P)	7.4×10^{4}	2.1×10^{-3}	$\mathbf{3.5\times10^{7}}$	1.9×10^{5}	1.9×10^{-3}	$\mathbf{1.0\times10^{8}}$	2.0×10^{5}	1.5×10^{-3}	$\mathbf{1.4\times10^{8}}$
A15(142S)	6.1×10^{4}	5.6×10^{-3}	$\mathbf{1.1\times10^{7}}$	6.3×10^{4}	3.8×10^{-3}	$\mathbf{1.6\times10^{7}}$	1.8×10^{5}	7.0×10^{-3}	$\mathbf{2.5\times10^{7}}$
A15(148I)	1.1×10^{5}	2.1×10^{-3}	$\mathbf{5.3\times10^{7}}$	7.0×10^{5}	2.3×10^{-3}	$\mathbf{3.0\times10^{8}}$	5.9×10^{5}	1.1×10^{-3}	$\mathbf{6.0\times10^{8}}$
A15(IF)	2.9×10^{5}	5.1×10^{-3}	$\mathbf{5.6\times10^{7}}$	6.4×10^{5}	1.7×10^{-3}	$\mathbf{3.8\times10^{8}}$		✕	
A15(IP)	1.6×10^{5}	2.6×10^{-3}	$\mathbf{5.9\times10^{7}}$		✕			✕	
A15(IS)	7.3×10^{4}	4.1×10^{-3}	$\mathbf{1.8\times10^{7}}$	2.8×10^{5}	1.0×10^{-3}	$\mathbf{2.8\times10^{8}}$		✕	
A15(II)	2.3×10^{5}	3.0×10^{-3}	$\mathbf{7.6\times10^{7}}$		✕			✕	
A15(FP)	1.1×10^{5}	8.5×10^{-3}	$\mathbf{1.3\times10^{7}}$		✕			✕	
A15(FS)	1.1×10^{5}	1.1×10^{-2}	$\mathbf{1.0\times10^{7}}$	3.6×10^{5}	5.9×10^{-4}	$\mathbf{6.0\times10^{8}}$		✕	
A15(FI)	2.6×10^{5}	8.4×10^{-4}	$\mathbf{3.0\times10^{8}}$		✕			✕	
A15(PS)		✕		2.0×10^{5}	7.9×10^{-4}	$\mathbf{2.5\times10^{8}}$		✕	
A15(PI)	1.5×10^{5}	3.5×10^{-3}	$\mathbf{4.0\times10^{7}}$		✕			✕	
A15(SI)	3.7×10^{4}	6.0×10^{-3}	$\mathbf{6.1\times10^{6}}$	2.0×10^{5}	7.0×10^{-4}	$\mathbf{2.9\times10^{8}}$		✕	
A15(IFP)		✕			✕			✕	
A15(IFS)	3.5×10^{4}	3.5×10^{-3}	$\mathbf{1.0\times10^{7}}$	7.6×10^{4}	1.8×10^{-3}	$\mathbf{4.3\times10^{7}}$		✕	
A15(IFI)	1.2×10^{5}	4.2×10^{-3}	$\mathbf{2.9\times10^{7}}$		✕			✕	
A15(IPS)	9.3×10^{4}	5.4×10^{-4}	$\mathbf{1.7\times10^{8}}$		✕			✕	
A15(IPI)		✕			✕			✕	
A15(ISI)	4.5×10^{4}	1.5×10^{-3}	$\mathbf{3.1\times10^{7}}$		✕			✕	
A15(FPS)	8.5×10^{4}	8.8×10^{-3}	$\mathbf{9.7\times10^{6}}$	2.0×10^{5}	4.2×10^{-4}	$\mathbf{4.8\times10^{8}}$		✕	
A15(FPI)	1.4×10^{5}	4.3×10^{-3}	$\mathbf{3.3\times10^{7}}$		✕			✕	
A15(FSI)	5.0×10^{4}	9.4×10^{-3}	$\mathbf{5.4\times10^{6}}$	4.6×10^{5}	1.6×10^{-3}	$\mathbf{1.6\times10^{8}}$		✕	
A15(PSI)	5.9×10^{4}	7.1×10^{-4}	$\mathbf{8.4\times10^{7}}$	4.0×10^{5}	2.9×10^{-4}	$\mathbf{1.4\times10^{9}}$		✕	
A15(IFPS)	1.5×10^{5}	4.2×10^{-3}	$\mathbf{3.6\times10^{7}}$		✕			✕	
A15(IFPI)	2.5×10^{5}	5.5×10^{-4}	$\mathbf{4.5\times10^{8}}$		✕			✕	
A15(IFSI)	1.3×10^{5}	1.7×10^{-3}	$\mathbf{7.7\times10^{7}}$	4.7×10^{5}	8.5×10^{-4}	$\mathbf{5.5\times10^{8}}$		✕	
A15(IPSI)	1.7×10^{5}	2.5×10^{-3}	$\mathbf{6.7\times10^{7}}$		✕			✕	
A15(FPSI)	8.6×10^{4}	6.1×10^{-3}	$\mathbf{1.4\times10^{7}}$		✕			✕	
A15(IFPSI)	2.1×10^{5}	2.2×10^{-4}	$\mathbf{9.8\times10^{7}}$		✕			✕	

Table 3.3 Kinetic SPR analysis of the peptides towards mAbs SD6, 4C4 and 3E5.

Notes:
Although resulting from apparently reliable data fits, kinetic parameters should be regarded with some caution, since most k_a values are in the limit for reliable kinetic measurements not affected by mass-transport limitations.
✕non-measurable interactions.

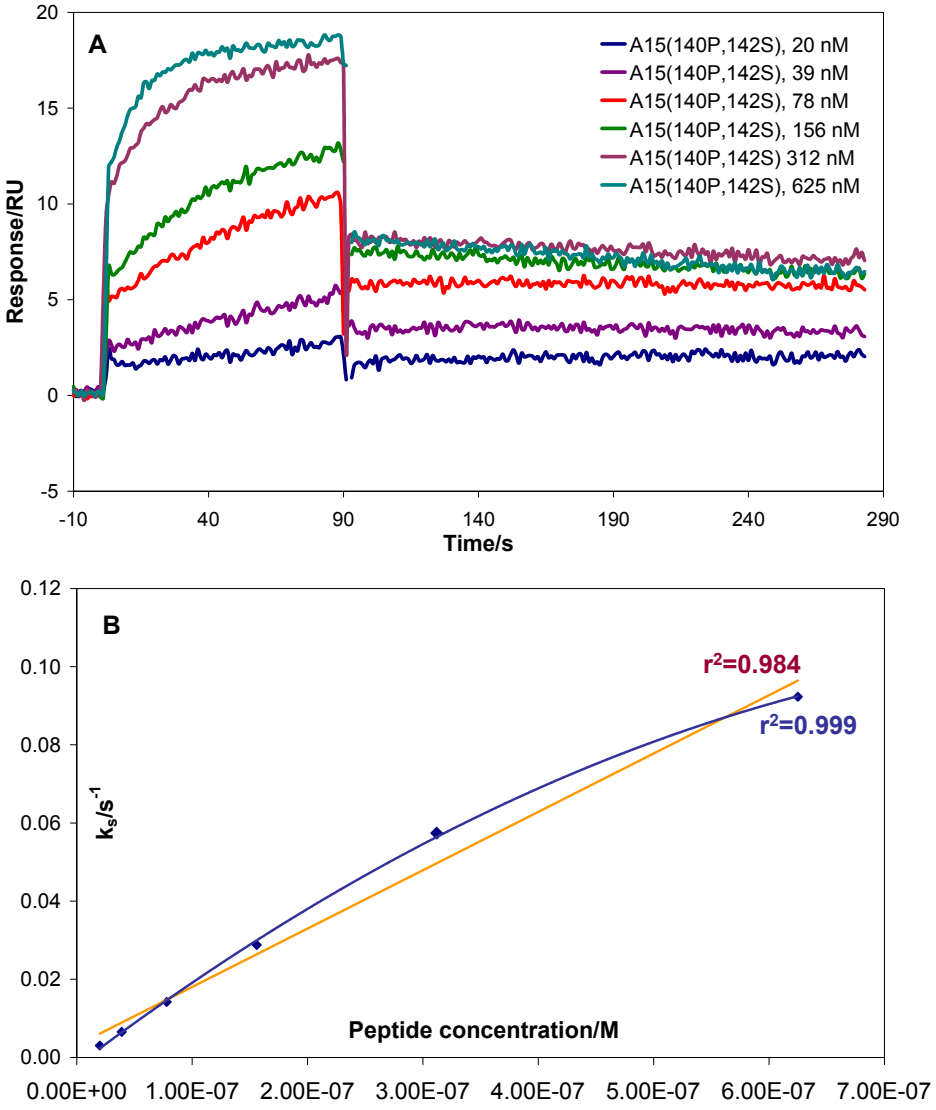

Figure 3. 3 Sensorgrams of the interaction between peptide A15(140P,142S) and mAb 4C4 (***A***); despite the good quality of data when using global curve fitting, slight deviations were observed in the dissociation rate constants (increasing with peptide concentration) when local curve fitting was employed; this fact together with the slight curvature observed when plotting k_s against peptide concentration (***B***) indicate that non-ideal effects were affecting binding kinetics.

3.3 Indirect SPR kinetic analysis using a high molecular weight competitor antigen[7]

As explained in section 0.2.3, there are indirect SPR methods for the kinetic characterisation of biospecific interactions between an immobilised receptor and small ligands in solution. One of them is a kind of surface competition assay, where a high molecular weight ligand, specific to the immobilised receptor, is injected and detected on the sensor chip surface. The kinetics of the macromolecular ligand – receptor interaction is characterised and, then, mixtures of this macromolecule with varying concentrations of the small analyte of interest are injected (Fig. 3.4). The effects observed on the macromolecule – receptor interaction upon addition of the small competitor analyte provide an indirect means to measure the kinetics of the small analyte – receptor interaction.

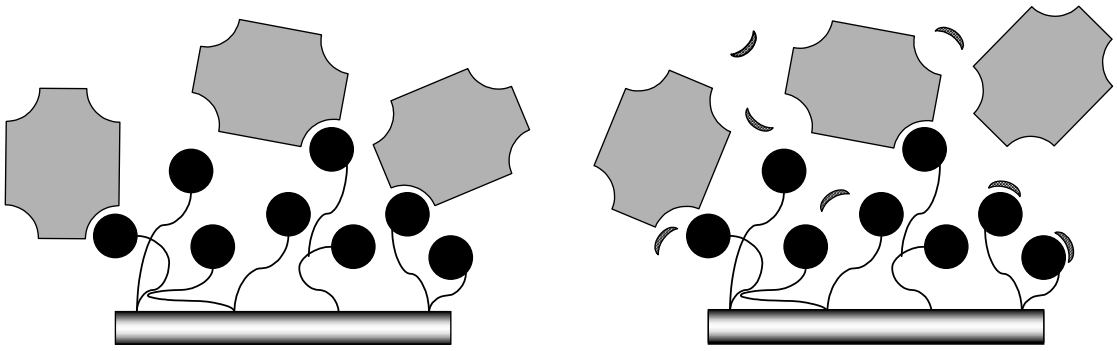

Figure 3. 4 Main steps in the surface competition SPR kinetic analysis: *left* – the kinetics of the interaction between surface – immobilised receptor (brown) and the macromolecular analyte (yellow) is measured; *right* – effects due to addition of a small competitor (target analyte, green) on the macromolecule – receptor interaction are evaluated and the kinetics of the small analyte – receptor interaction is thus determined.

Due to problems often observed in the direct kinetic SPR described in the previous section, it was thought that perhaps an indirect approach would be more appropriate. Indeed, peptide – antibody interactions seemed to be affected by diffusion-controlled kinetics, due to the apparently high association rates involved. Further, symptoms of both analyte rebinding and surface saturation at higher analyte concentrations were equally observed. Thus, it would seem advisable to decrease mAb surface density and analyte concentrations as much as possible, in order to minimise such non-ideal effects[4-6]. However, this would imply severe losses in response levels, given the small size of the target analytes. Therefore, an indirect approach based on the detection of a macromolecular analyte would be a possible solution for these problems[7].

In the absence of a natural macromolecular FMDV antigen available for such surface competition SPR assays, alternative high molecular weight antigens were chosen, as described in the following sections.

3.3.1 Peptide – protein (1:1) conjugate: the A15 – human carbonic anhydrase I (HCA I) construct

To ensure unambiguous mechanisms for peptide – macromolecule competitive binding to the antibody paratope, a macromolecular antigen with only one specific epitope *per* molecule was needed. This implied the conjugation of a site A representative peptide such as A15 to a protein carrier in a 1:1 stoichiometry. A safe way to achieve such stoichiometry would be to link through a heterodisulphide bond the A15 sequence (with an additional Cys residue) to a carrier protein bearing a single Cys.

Search in the Protein Data Bank for a protein suitable for such purposes (*i.e.*, with a single cysteine residue, weighing over *ca.* 10 kDa, commercially available and affordable) led to human carbonic anhydrase I (HCA I – E. C. 4.2.1.1).

3.3.1.1 Synthesis of peptide (Npys)Cys – A15 and heterodimerisation with protein HCA I

The A15 sequence was assembled as described in previous sections, then Boc–Cys(Npys)–OH was coupled as N-terminal residue by similar protocols and cleavage/side chain deprotection with TFA was then performed as usual (see Materials & Methods, section 4.3), leading to peptide (Npys)Cys–A15 (Table 3.4). The 3-nitro-2-pyridylsulphenyl (Npys) group is stable to TFA and therefore not removed in the cleavage. This thiol protecting group was chosen for its well-known applicability to direct peptide – protein conjugation through cysteine residues. Such property of the Npys group is due both to the fact that it is stable to the standard acidolytic cleavage conditions (even to hydrogen fluoride acidolysis in Boc/Bzl chemistry) and also to its thiol-activating character, which allows regiospecific peptide – protein coupling through cysteine residues (Fig. 3.5)[8].

Table 3.4 General data concerning the synthesis of peptide (Npys)Cys – A15.

Global yield (%)	***Purity (% HPLC)***	***MW found***	***MW expected***	***AAA***
67	81	1833.6	1833	Asp, 1.04 (1); Ser, 0.93 (1); Gly, 1.07 (1); Ala, 3.10 (3); Leu, 2.00 (2); His, 0.97 (1)

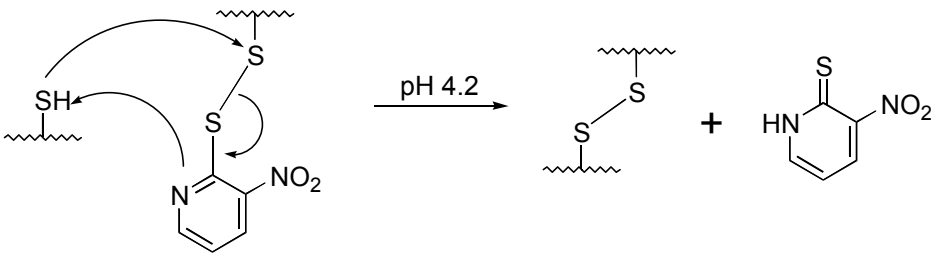

Figure 3. 5 Regiospecific formation of a disulphide heterodimer *via* the Npys thiol activation; Npys not only serves as thiol-protection during peptide synthesis, but also activates the Cys sulphur atom toward other nucleophiles, such as other Cys thiol groups[8].

The heterodimerisation reaction was carried out overnight under acidic, denaturating conditions (6 M guanidine hydrochloride in water, pH 4.2) using excess peptide, and was monitored by HPLC (Fig. 3.6). The final reaction mixture was dialysed (MW cut-off = 15 to 20 kDa) against decreasing concentrations of guanidine hydrochloride in water for 48 hours. The major product in the final dialysed solution was characterised by MALDI-TOF MS (Fig. 3.7) as the target HCA I – CysA15 1:1 conjugate.

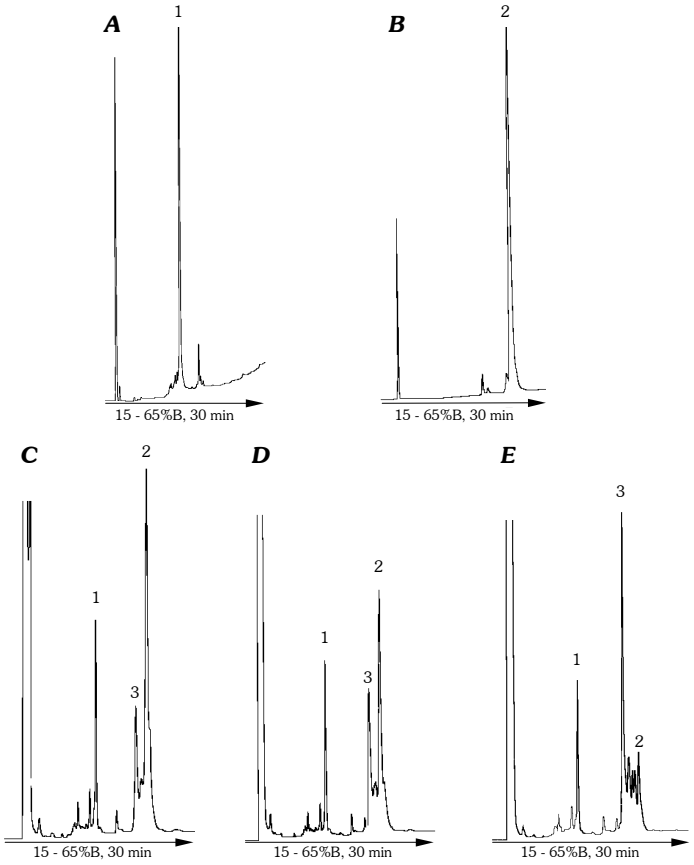

Figure 3. 6 HPLC monitoring of the heterodimerisation reaction: ***A***. crude (Npys)Cys – A15 peptide; ***B***. HCA I; ***C***, ***D*** and ***E*** progress of the reaction at 2, 8 and 24 h, respectively.

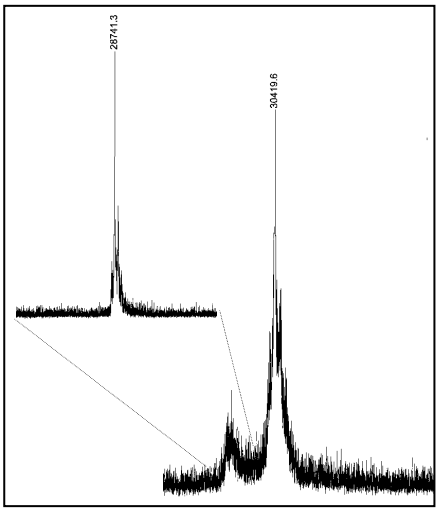

Figure 3. 7 MALDI-TOF MS spectrum of the final heterodimerisation product, which contains unreacted HCA I protein (the MALDI-TOF MS spectrum of the commercial HCA I is shown in the upper left corner).

3.3.1.2 Antigenic evaluation of the HCA I – CysA15 conjugate

The adequacy of the HCA I – CysA15 construct as an FMDV antigen was evaluated by direct SPR detection on SD6, 4C4 and 3E5 surfaces (with mAb densities of approximately 600 RU, *i. e*, 0.6 ng/mm^2). Unfortunately, absence of specific response was repeatedly observed, showing that the construct was not antigenic towards these mAbs (Fig. 3.8). Some assays at pH values (5.8 and 8) different from the usually employed (7.3) did not improve the results (only non-specific binding between protonated protein – negatively-charged dextran layer was observed at the lowest pH).

These results were confirmed by competition ELISA experiments using A21 – KLH conjugate as the plate-bound antigen (Fig. 3.9). Inadequate conformational presentation or inaccessibility of peptide A15 were considered as probable causes for such lack of antigenicity.

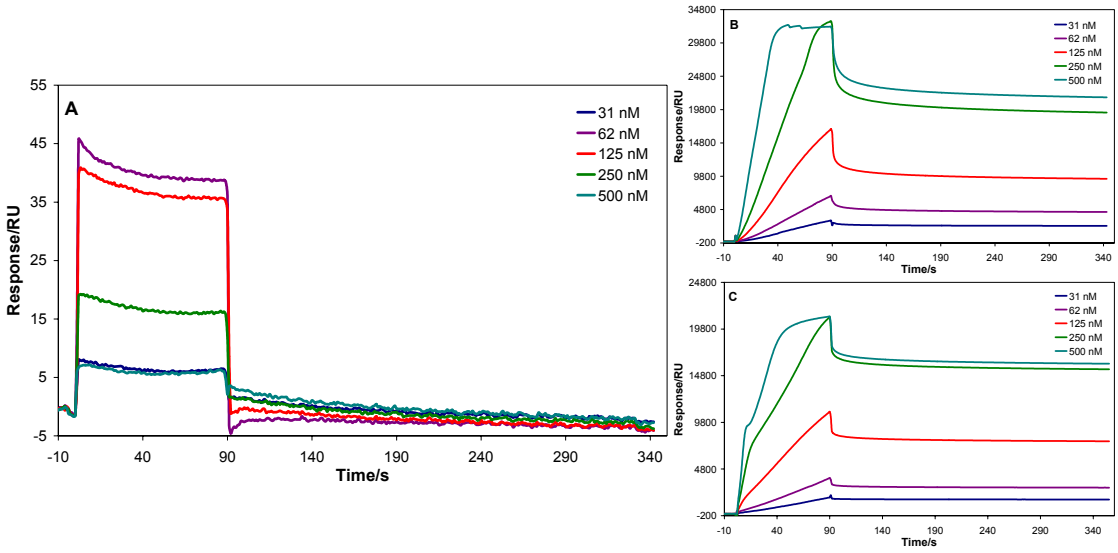

Figure 3. 8 SPR analysis of conjugate HCA I – CysA15: ***A***. injection of conjugate samples over a mAb 4C4 surface (600 RU), employing the conditions used for FMDV peptides; ***B***. and ***C***. injection of protein samples at pH 5.8 over the same 4C4 surface and over an non-derivatised sensor chip surface, respectively.

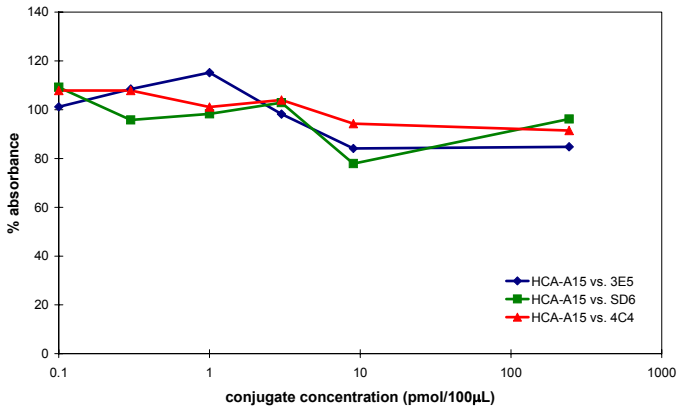

Figure 3. 9 Inhibition curves from competition ELISA analysis of the HCA I – CysA15 conjugate (curves for reference peptide A15 were omitted).

3.3.2 Recombinant engineered proteins bearing the FMDV GH loop peptide: protein JX249A

3.3.2.1 Preliminary assays

The extensive research work on recombinant proteins bearing the FMDV C-S8c1 GH loop carried out by A. Villaverde and co-workers[9-12] opened the possibility to use one of these engineered proteins as such macromolecular antigen.

A recombinant β-galactosidase from *Escherichia coli,* protein JX249A, has solvent exposed-loops which have been engineered for the insertion of a peptide from the GH loop of FMDV C-S8c1 (TT***[136]YTASARGDLAHLTT[150]T***HARHLP). JX249A is a homotetramer with four GH loops *per* protein, having a total molecular weight of 472 kDa. Given its high antigenicity, JX249A was tested in preliminary SPR assays[A], where each protein molecule would be regarded as four independent antigenic monomers to simplify data processing. The first assays confirmed the antigenicity of JX249A towards mAbs SD6, 4C4 and 3E5, and preliminary analyses also indicated that peptide A15 competed with JX249A in binding to surface-immobilised mAb (surface densities of about 600 RU), while non-specific peptide A15Scr did not (Fig. 3.10). Nevertheless, important problems due to insufficient surface regeneration and consequent protein accumulation on the surface led to short surface life-times and prevented a systematic screening of the peptide antigens.

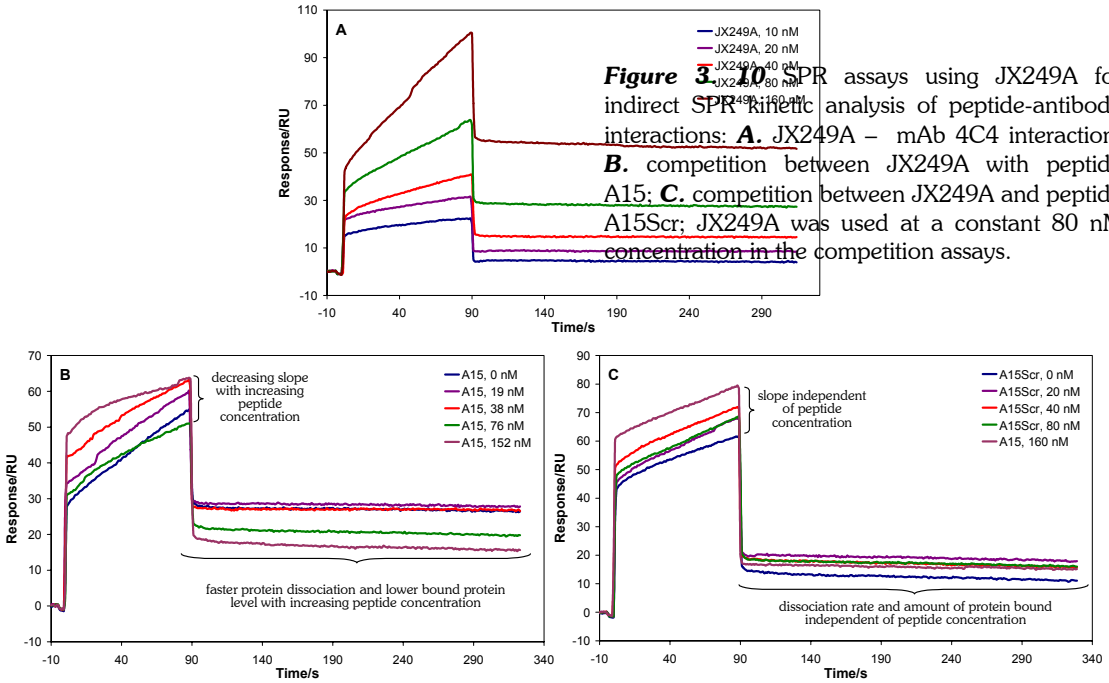

Figure 3.10 SPR assays using JX249A for indirect SPR kinetic analysis of peptide-antibody interactions: ***A.*** JX249A – mAb 4C4 interaction; ***B.*** competition between JX249A with peptide A15; ***C.*** competition between JX249A and peptide A15Scr; JX249A was used at a constant 80 nM concentration in the competition assays.

[A] Protein engineering, production and antigenic evaluation by ELISA were performed by Dr. A. Villaverde and co-workers (U. A. B., Bellaterra – Barcelona), who kindly offered protein samples to the author.

3.3.2.2 Screening of alternative regeneration conditions

Insufficient surface regeneration was, once again, preventing the study of the kinetics of peptide – mAb interactions by SPR. Therefore, a study of regeneration conditions, as described by Andersson and co-workers[13], was carried out. This study was based on the screening of several regeneration cocktails, consisting of mixtures of the stock solutions presented in Table 3.5. This multi-cocktail approach is based on the principle that what one kind of chemical property (acidic, basic, saline, organic, denaturating) cannot disrupt, perhaps another one can or, even better, combination of several distinct chemical properties will act synergistically and solve the regeneration problem.

Table 3.5 Stock solutions[13]used for the multi-cocktail surface regeneration approach in SPR analysis.

Cocktail	***Main chemical properties***	***Composition***
A	Acid	Equal volumes of 0.15 M phosphoric, formic and malonic acids, adjusted to pH 5 with 4 M NaOH
B	Basic	Equal volumes of 0.20 M ethanolamine, sodium phosphate, piperazine and glycine, adjusted to pH 9 with 2 M HCl
I	Ionic/denaturating	Potassium thiocianate (0.46 M), magnesium chloride (1.83 M), urea (0.92 M) and guanidine hydrochloride (1.83 M)
U	Non-polar/organic	Equal volumes of dimethylsulfoxide, formamide, acetonitrile, ethanol and 1-butanol
D	Detergent	0.3% (w/w) CHAPS, 0.3% (w/w) zwittergent 3-12, 0.3% (v/v) Tween 80, 0.3% (v/v) Tween 20 and 0.3% (v/v) Triton X-100
C	Chelating	20 mM EDTA aqueous solution

The general protocol consists of a screening and an optimisation step. In the first step, diluted solutions or simple binary combinations of the above described cocktails are tested (Table 3.6). The evaluation of the screening cocktails is carried out in the biosensor and, afterwards, an optimisation step is performed upon combinatorial mixing of the stock cocktails rated as the best.

Table 3.6 Cocktails used in the screening step of the multi-cocktail regeneration approach[13].

Composition of the screening cocktails
Bww Iww Dww Uww Cww BDw BCw Aiw Adw Auw Acw Idw Icw Duw DCw Ucw ABw

* equivalent amounts (v/v) of each cocktail represented by the corresponding letter (see Table 3.5); w stands for water.

Having an immunoglobulin as the surface-immobilised receptor, the use of cocktails I or D, as defined in Table 3.5, could be harmful. Therefore, cocktails A, B, C, U and a modified ionic cocktail I' (differing from I in that denaturating chemicals such as urea or guanidine hydrochloride were not added) were screened as described. The screening was performed on high density mAb surfaces (*ca.* 3 ng/mm^2) to ensure high responses for an unequivocal evaluation of the cocktail regeneration efficacy. In neither case was a significant improvement observed (Fig. 3.11).

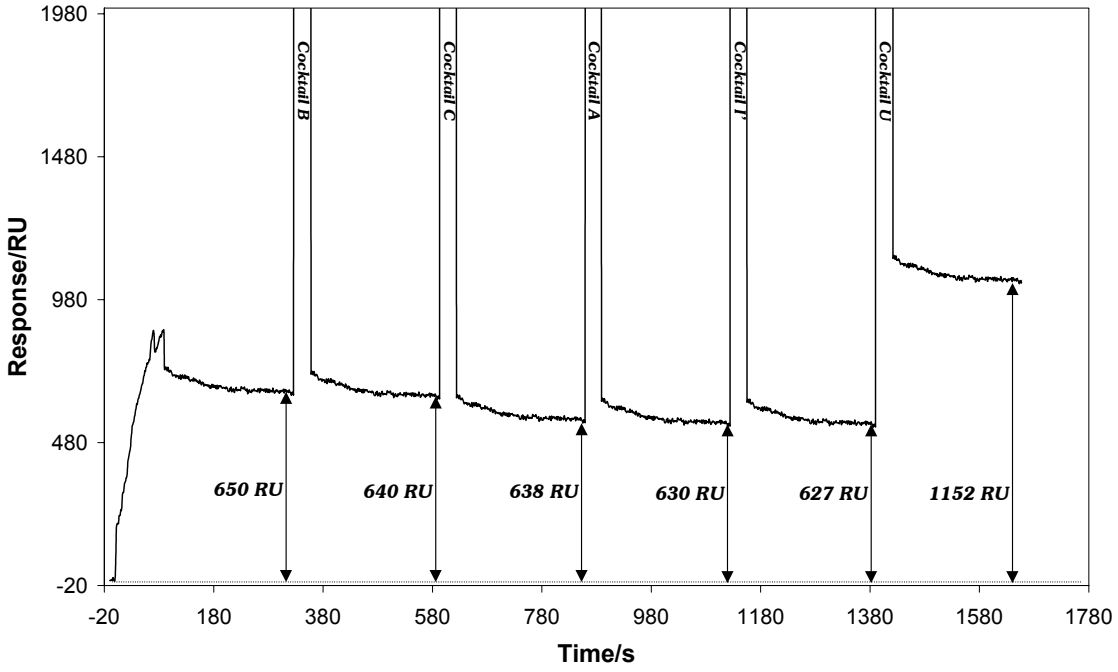

Figure 3. 11 Successive injections of stock regeneration solutions Bww, Cww, Aww, I'ww and Uww (see Table 3.6) on a mAb 4C4 surface (3 ng/mm^2), after binding of protein JX249A (300 nM).

Results in Fig. 3.11 show the inefficacy of the stock regeneration solutions tested for recovering the initial baseline level. Further tests, either with triplicate injections of each regeneration cocktail or with binary combinations of the stock solutions (AI' and CI' at different proportions), did not improve the results. The increase in response level observed when injecting cocktail Uww was attributed to compression of the hydrophilic dextran matrix due to the organic solvents present in this cocktail.

The cocktail approach was also tested on some problematic peptide – mAb interactions (mentioned in 3.2), but results were none the better.

3.3.2.3 Capping of JX249A free cysteine thiol groups

We hypothesised that the free thiol groups from the JX249A cysteine residues might be the source for the irreversible binding of the protein to the mAb surfaces, upon disulphide bridge cross-linking. Usually, experiments with bacterial β-galactosidases at room temperature require the addition of β-mercaptoethanol, in order to maintain the cysteine thiol groups in their native free form and to avoid protein aggregation. In the above SPR experiments, β-mercaptoethanol was not added, since protein solutions would be put in contact with an antibody surface and native folding of the immunoglobulin had to be preserved. Thus, capping of the JX249A cysteine thiol groups seemed to be a wise precaution to avoid both protein aggregation and, possibly, disulphide cross-linking to the mAb surfaces.

Capping of the free thiol groups was carried out by nucleophilic substitution with iodoacetic acid (Fig. 3.12) as described under Materials & Methods (section 4.3); this converted cysteine residues into carboxymethylcysteine[14]. Protein integrity after carboxymethylation was checked by SDS-PAGE (Fig. 3.13) and capping yield (75%) was assessed by AAA, using carboxymethylcysteine standards.

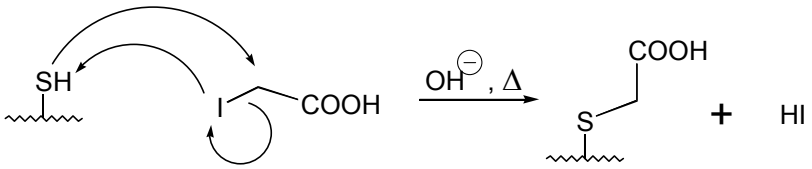

Figure 3. 12 Nucleophilic attack of a thiol sulphur atom on the methylene group of iodoacetic acid[14].

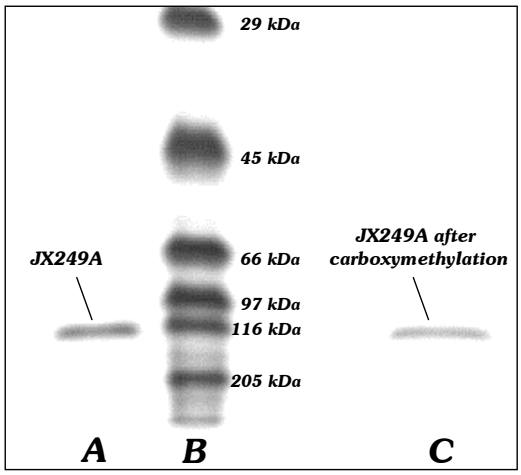

Figure 3. 13 SDS-PAGE (10% acrylamide) analysis of protein JX249A before (lane A) and after (lane C) carboxymethylation of the cysteine side-chain thiol groups; the following protein standards (lane B) were employed: from higher to lower MW – myosin, β-galactosidase, phosphorylase B, bovine albumin, ovalbumin and carbonic anhydrase.

Use of the capped JX249A in SPR assays as those described in the previous section did not, unfortunately, solve the regeneration problems already observed (not shown). This indicated that such problems were due either to intrinsic features of the protein – surface interactions or to the presence of some free JX249A mixed with the carboxymethylated protein.

3.4 Solution affinity SPR analysis of the peptide antigens

Several features of anti-FMDV mAb interactions with either the peptide antigens or protein JX249A prevented their dynamic characterisation by means of SPR kinetic analysis. Therefore, the characterisation of the synthetic peptides under study was alternatively carried out by solution affinity SPR analysis[15,16], as previously described for the FMDV C-S30 peptides (previous chapter, section 2.7). The same experimental set-up was employed under similar conditions (described in Materials & Methods, section 4.3). A confirmative competition ELISA screening of the peptides was carried out in parallel, as described in section 2.3.

Inhibition curves such as those exemplified in Fig. 3.14 were observed and affinity constants were determined by the Cheng & Prusoff's formula[17], as previously exposed in section 2.7. These constants are presented in Table 3.7, where the corresponding results from kinetic SPR analysis and competition ELISA are included, for comparison purposes.

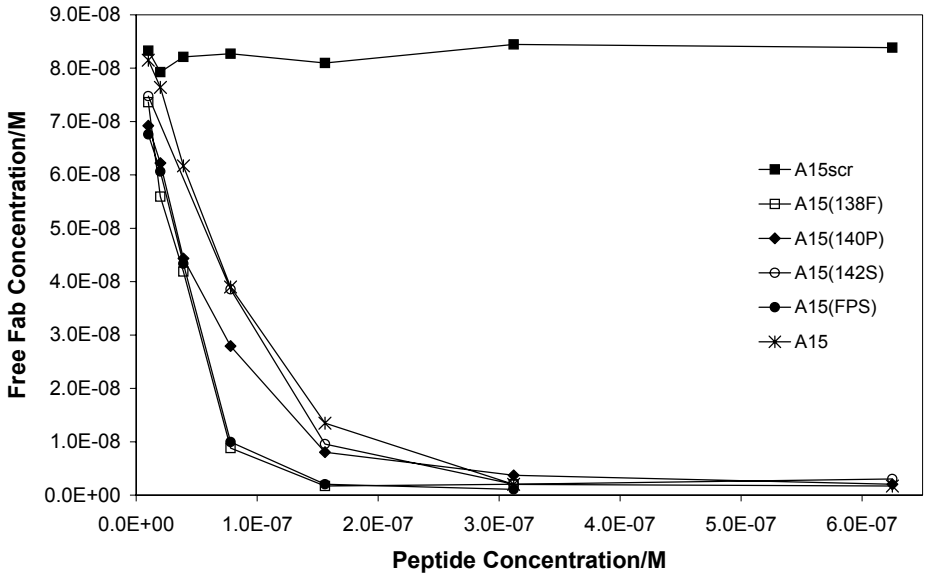

Figure 3. 14 Inhibition curves in the SPR analysis of the interactions between Fab 4C4 and peptide antigens in solution; a constant 80 nM total concentration of Fab was employed; peptide A15Scr was included as a negative control.

Analysis of quantitative data in Table 3.7 shows that all the peptides are highly antigenic, taking the native A15 antigen as reference. Differences observed between SPR data in kinetic or in solution equilibrium experiments were not generally significant. This is a further evidence of the reliability of the kinetic SPR methodology employed along the present study of FMDV peptides. More pronounced differences were due either to mass transport-influenced kinetic data or to the fact that immobilised mAb – free peptide and free mAb – free peptide interactions are intrinsically different and therefore only peptide ranking should be compared.

Table 3.7 Affinity constants for the interactions between mAbs (Fab) SD6, 4C4 and 3E5 with the peptide antigens bearing combinations of the replacements Thr137→Ile, Ala138→Phe, Ala140→Pro, Gly142→Ser and Thr148→Ile (columns labelled $K_{A\text{-}sol.aff.}$).

Fab / *Peptide*	***SD6***			***4C4***			**3E5**		
	$K_{A\text{-}sol.aff.}/M^{-1}$	$K_{A\text{-}kin}/M^{-1}$	***E***	$K_{A\text{-}sol.aff.}/M^{-1}$	$K_{A\text{-}kin}/M^{-1}$	***E***	$K_{A\text{-}sol.aff.}/M^{-1}$	$K_{A\text{-}kin}/M^{-1}$	***E***
A15	$\mathbf{6.3\times10^{7}}$	5.4×10^{7}	++	$\mathbf{2.0\times10^{8}}$	1.9×10^{8}	++	$\mathbf{2.0\times10^{8}}$	9.4×10^{7}	++
A15(137I)	$\mathbf{8.5\times10^{7}}$	1.9×10^{8}	++	$\mathbf{2.0\times10^{8}}$	1.4×10^{8}	++	$\mathbf{1.4\times10^{8}}$	3.4×10^{8}	++
A15(138F)	$\mathbf{3.6\times10^{7}}$	2.2×10^{7}	++	$\mathbf{2.1\times10^{8}}$	9.8×10^{7}	++	$\mathbf{2.1\times10^{8}}$	4.0×10^{8}	++
A15(140P)	$\mathbf{7.1\times10^{7}}$	3.5×10^{7}	++	$\mathbf{1.8\times10^{8}}$	1.0×10^{8}	++	$\mathbf{1.6\times10^{8}}$	1.4×10^{8}	++
A15(142S)	$\mathbf{2.7\times10^{7}}$	1.1×10^{7}	++	$\mathbf{7.3\times10^{7}}$	1.6×10^{7}	++	$\mathbf{6.2\times10^{7}}$	2.5×10^{7}	++
A15(148I)	$\mathbf{6.7\times10^{7}}$	5.3×10^{7}	++	$\mathbf{2.0\times10^{8}}$	3.0×10^{8}	++	$\mathbf{2.0\times10^{8}}$	6.0×10^{8}	++
A15(IF)	$\mathbf{5.1\times10^{7}}$	5.6×10^{7}	++	$\mathbf{2.2\times10^{8}}$	3.8×10^{8}	++	$\mathbf{1.6\times10^{8}}$	✕	++
A15(IP)	$\mathbf{6.1\times10^{7}}$	5.9×10^{7}	++	$\mathbf{2.1\times10^{8}}$	✕	++	$\mathbf{1.3\times10^{8}}$	✕	++
A15(IS)	$\mathbf{5.2\times10^{7}}$	1.8×10^{7}	++	$\mathbf{1.9\times10^{8}}$	2.8×10^{8}	++	$\mathbf{1.3\times10^{8}}$	✕	++
A15(II)	$\mathbf{9.1\times10^{7}}$	7.6×10^{7}	++	$\mathbf{2.3\times10^{8}}$	✕	++	$\mathbf{2.0\times10^{8}}$	✕	++
A15(FP)	$\mathbf{2.8\times10^{7}}$	1.3×10^{7}	++	$\mathbf{2.2\times10^{8}}$	✕	++	$\mathbf{2.0\times10^{8}}$	✕	++
A15(FS)	$\mathbf{7.1\times10^{6}}$	1.0×10^{7}	++	$\mathbf{2.0\times10^{8}}$	6.0×10^{8}	++	$\mathbf{1.6\times10^{8}}$	✕	++
A15(FI)	$\mathbf{2.1\times10^{7}}$	3.0×10^{8}	++	$\mathbf{2.1\times10^{8}}$	✕	++	$\mathbf{1.9\times10^{8}}$	✕	++
A15(PS)	$\mathbf{3.6\times10^{7}}$	✕	++	$\mathbf{2.0\times10^{8}}$	2.5×10^{8}	++	$\mathbf{6.2\times10^{7}}$	✕	++
A15(PI)	$\mathbf{6.0\times10^{7}}$	4.0×10^{7}	++	$\mathbf{1.8\times10^{8}}$	✕	++	$\mathbf{1.9\times10^{8}}$	✕	++
A15(SI)	$\mathbf{1.6\times10^{7}}$	6.1×10^{6}	++	$\mathbf{1.9\times10^{8}}$	2.9×10^{8}	++	$\mathbf{1.2\times10^{8}}$	✕	++
A15(IFP)	$\mathbf{7.4\times10^{7}}$	✕	++	$\mathbf{2.2\times10^{8}}$	✕	++	$\mathbf{1.9\times10^{8}}$	✕	++
A15(IFS)	$\mathbf{2.0\times10^{7}}$	1.0×10^{7}	++	$\mathbf{8.5\times10^{7}}$	4.3×10^{7}	++	$\mathbf{5.9\times10^{7}}$	✕	++
A15(IFI)	$\mathbf{5.6\times10^{7}}$	2.9×10^{7}	++	$\mathbf{2.4\times10^{8}}$	✕	++	$\mathbf{1.8\times10^{8}}$	✕	++
A15(IPS)	$\mathbf{7.4\times10^{7}}$	1.7×10^{8}	++	$\mathbf{2.2\times10^{8}}$	✕	++	$\mathbf{1.4\times10^{8}}$	✕	++
A15(IPI)	$\mathbf{7.9\times10^{7}}$	✕	++	$\mathbf{2.2\times10^{8}}$	✕	++	$\mathbf{2.0\times10^{8}}$	✕	++
A15(ISI)	$\mathbf{4.5\times10^{7}}$	3.1×10^{7}	++	$\mathbf{2.2\times10^{8}}$	✕	++	$\mathbf{1.7\times10^{8}}$	✕	++
A15(FPS)	$\mathbf{6.5\times10^{6}}$	9.7×10^{6}	++	$\mathbf{2.1\times10^{8}}$	4.8×10^{8}	++	$\mathbf{1.3\times10^{8}}$	✕	++
A15(FPI)	$\mathbf{5.0\times10^{7}}$	3.3×10^{7}	++	$\mathbf{1.3\times10^{8}}$	✕	++	$\mathbf{1.8\times10^{8}}$	✕	++
A15(FSI)	$\mathbf{1.3\times10^{7}}$	5.4×10^{6}	++	$\mathbf{2.1\times10^{8}}$	1.6×10^{8}	++	$\mathbf{1.5\times10^{8}}$	✕	++
A15(PSI)	$\mathbf{2.5\times10^{7}}$	8.4×10^{7}	++	$\mathbf{2.1\times10^{8}}$	1.4×10^{9}	++	$\mathbf{1.5\times10^{8}}$	✕	++
A15(IFPS)	$\mathbf{4.7\times10^{7}}$	3.6×10^{7}	++	$\mathbf{2.2\times10^{8}}$	✕	++	$\mathbf{1.3\times10^{8}}$	✕	++
A15(IFPI)	$\mathbf{7.1\times10^{7}}$	4.5×10^{8}	++	$\mathbf{2.0\times10^{8}}$	✕	++	$\mathbf{1.8\times10^{8}}$	✕	++
A15(IFSI)	$\mathbf{1.9\times10^{7}}$	7.7×10^{7}	++	$\mathbf{2.1\times10^{8}}$	5.5×10^{8}	++	$\mathbf{1.2\times10^{8}}$	✕	++
A15(IPSI)	$\mathbf{5.0\times10^{7}}$	6.7×10^{7}	++	$\mathbf{1.5\times10^{8}}$	✕	++	$\mathbf{1.3\times10^{8}}$	✕	++
A15(FPSI)	$\mathbf{1.7\times10^{7}}$	1.4×10^{7}	++	$\mathbf{2.2\times10^{8}}$	✕	++	$\mathbf{1.3\times10^{8}}$	✕	++
A15(IFPSI)	$\mathbf{3.8\times10^{7}}$	9.8×10^{7}	++	$\mathbf{1.9\times10^{8}}$	✕	++	$\mathbf{1.7\times10^{8}}$	✕	++

Note: values measured by kinetic SPR are included in columns labelled $\boldsymbol{K_{A\text{-}kin}}$; total Fab concentrations were kept constant for each peptide dilution series and peptide concentrations varied between 0 and 625nM; results from a competition ELISA screening of the peptides are also included (column E), where signs **–** , **+** and **++** stand for low (IC_{50} rel>30), medium ($30<IC_{50}$rel<10) and high antigenicity (IC_{50} rel<10), respectively.

The one-point mutants are closely equivalent regarding antigenicity. In spite of this, mAb SD6 slightly "resents" mutations A138→F and G142→S, while the other two mAbs only disfavour the mutation within the RGD motif. The higher involvement of residue 138 in peptide-SD6 complexes and the important role of the RGD triplet are both in agreement with these observations[1,18-21]. All mAbs are "indifferent" to mutations T137→I and T148→I, which is consistent with the almost absent participation of these residues in the mAb-peptide interactions[21].

Generally, the multiply substituted peptides displayed similar affinities, close to those expected from additive effects in the combination of the one-point mutations (Fig. 3.15). However, for mAbs 4C4 and 3E5, affinities of multiple mutants containing the G142→S replacement were systematically superior to those expected from the "additivity rule". Unless there was an undetected error in the affinities of all peptides containing this mutation towards both 4C4 and 3E5, these differences suggest a small positive synergistic effect in these multiple mutants. So it seems that mutations outside the RGD triplet compensate the slight decrease in affinity provoked by replacing glycine by serine in this important motif. Possibly, such compensation comes from peptide conformational features, which are not as favourable in the A15(142S) single-point mutant as when the other replacements are combined with the RSD motif.

Interestingly, peptides including multiple mutations within the GH loop of C-S8c1 FMDV still display antigenicities as high as those of the native sequence. This is even more relevant when one of these mutations is located in the RGD triplet and involves the substitution of a glycine by a serine residue. For these reasons, the multiply substituted peptide A15(FPS) was submitted to further structural studies, both by two-dimensional ^{1}H-NMR of free peptide in solution and by X-ray diffraction crystallography of its complex with antibody 4C4. Peptide A15(FPS) was chosen since it combines the three more relevant mutations. Also, W. F. Ochoa and co-workers have observed very low electron densities for residues placed at both ends of FMDV pentadecapeptides (residues≤137 and ≥148) preventing the unequivocal location of such residues in the structure of peptide-4C4 complexes. This has been interpreted as due to the lack of strong interactions between the terminal residues and the antibody paratope[21].

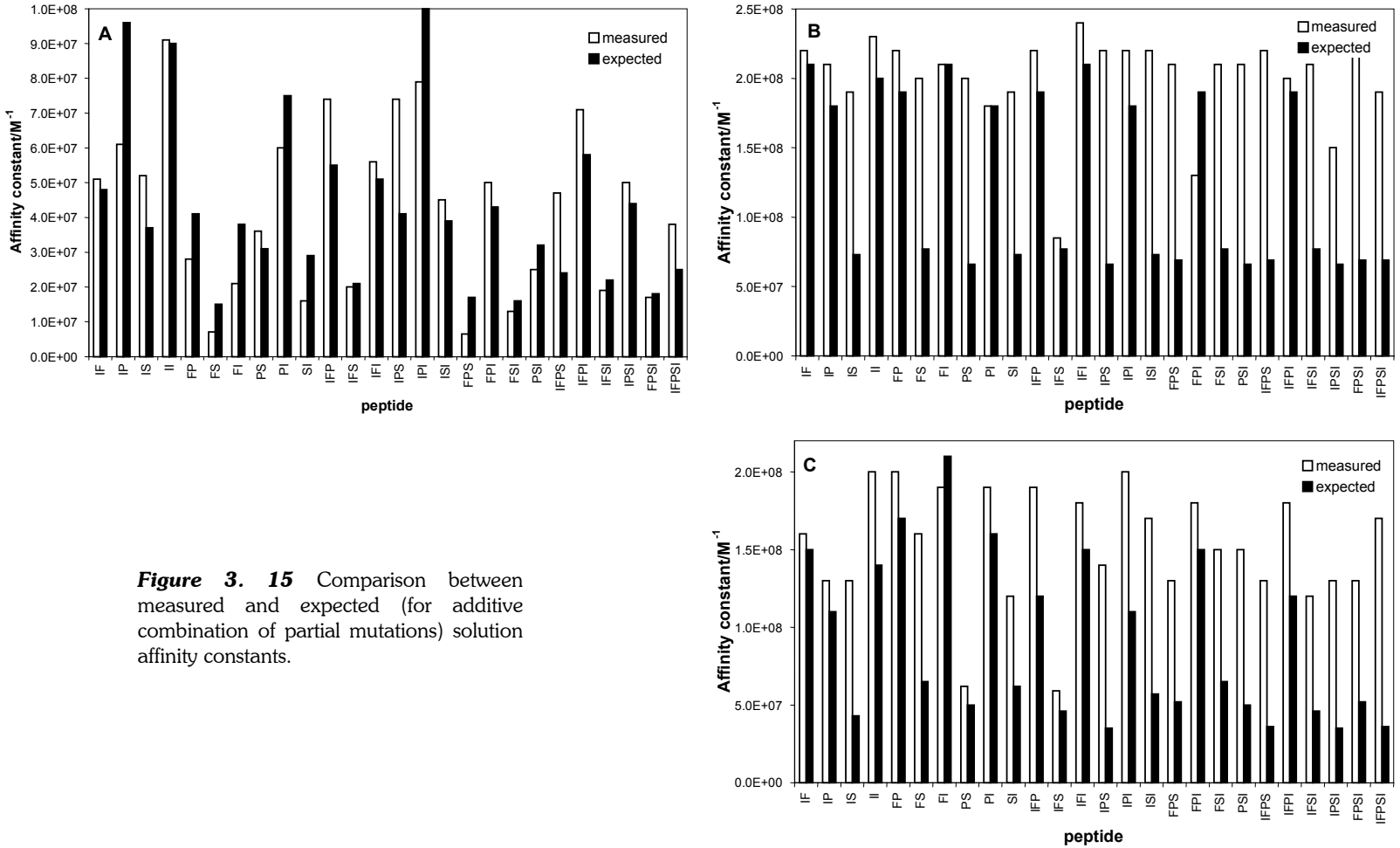

Figure 3. 15 Comparison between measured and expected (for additive combination of partial mutations) solution affinity constants.

3.5 Two-dimensional ^{1}H-NMR analysis of peptide A15(FPS)

The structural features of peptide A15(FPS) in solution were analysed by 2D – ^{1}H NMR[22], under conditions identical to those described in section 2.8 for C-S30 peptides. In the present case, peptide A15(FPS) was studied both in water and in 30% TFE, through TOCSY and NOESY/ROESY experiments (Fig. 3.16)[23-25]. The chemical shifts measured are presented in Table 3.8.

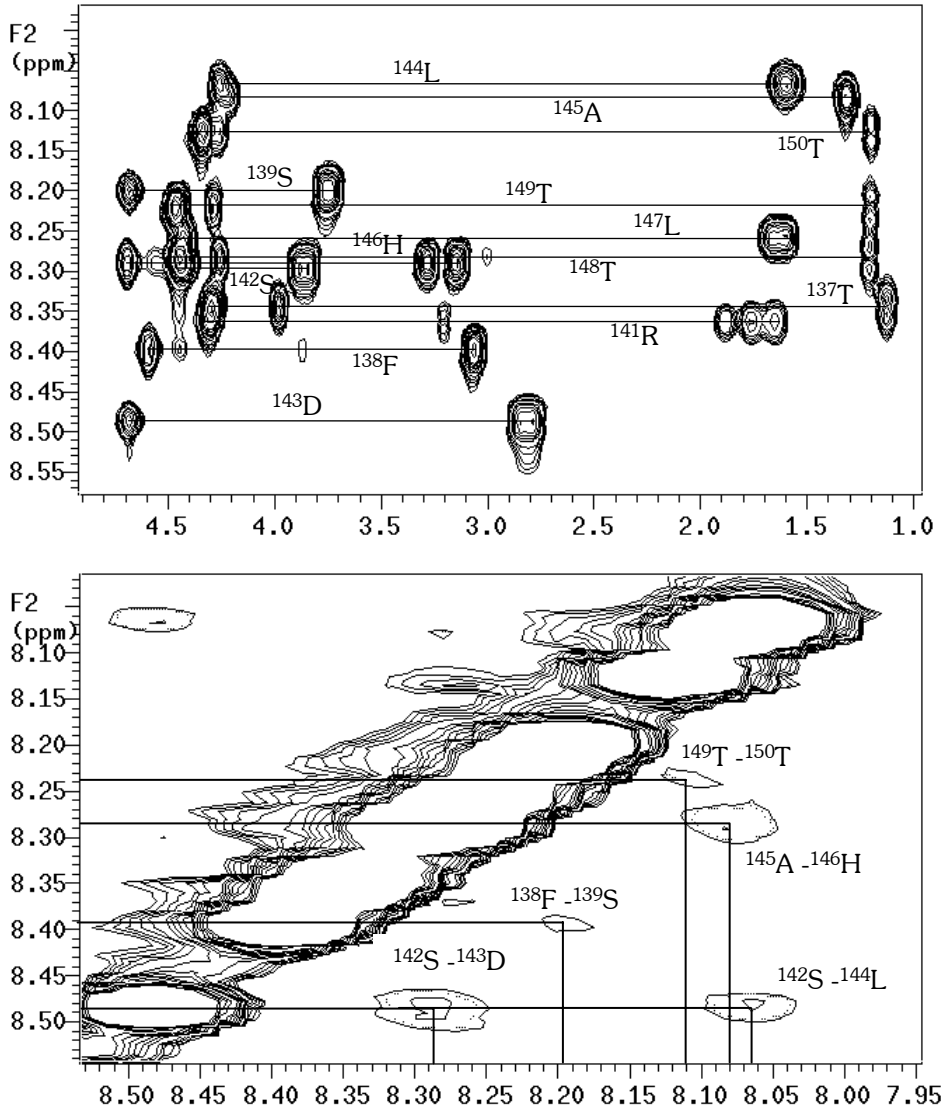

Figure 3. 16 Expansions of the TOCSY (above) and ROESY at 200 ms (below) spectra of peptide A15(FPS) in water at 25 °C.

Table 3.8 Chemical shifts measured in the 2D ^{1}H-NMR analysis of of peptide A15(FPS) at 25 °C.

Residue	***A15(FPS)***							
	H_2O				***30% TFE***			
	H^N	H^α	H^β	Other	H^N	H^α	H^β	Other
^{136}Tyr		4.23	3.03	7.14 6.80		4.23	3.05	7.04 6.84
^{137}Thr	8.34	4.28	4.22	1.12	8.25	4.34	4.03	1.16
^{138}Phe	8.39	4.58	3.07	7.29	8.24	4.64	3.09	7.30
^{139}Ser	8.20	4.68	3.75		8.04	4.76	3.84 3.78	
^{140}Pro		4.36	2.30 1.95	1.90 3.67 3.60		4.38	2.30 1.99	3.73 3.57
^{141}Arg	8.35	4.30	1.86 1.75	1.65 3.20 7.31	8.03	4.28	1.90 1.77	1.68 3.22 7.36
^{142}Ser	8.29	4.40	3.90 3.85		8.06	4.37	3.97 3.89	
^{143}Asp	8.49	4.68	2.85 2.80		8.34	4.66	2.85	
^{144}Leu	8.07	4.26	1.60	0.90 0.85	8.01	4.23	1.70 1.62	0.93 0.88
^{145}Ala	8.08	4.25	1.30		7.96	4.17	1.38	
^{146}His	8.29	4.69	3.27 3.15	7.60 7.18	8.04	4.63	3.38 3.24	8.06 7.33
^{147}Leu	8.25	4.42	1.60	0.90 0.85	8.07	4.36	1.78 1.66	0.93 0.90
^{148}Thr	8.28	4.45	4.25	1.26	7.98	4.42	4.34	1.26
^{149}Thr	8.23	4.46	4.30	1.20	7.93	4.47	4.28	1.25
^{150}Thr	8.12	4.33	4.28	1.20	*ambiguous due to peak overlap*			

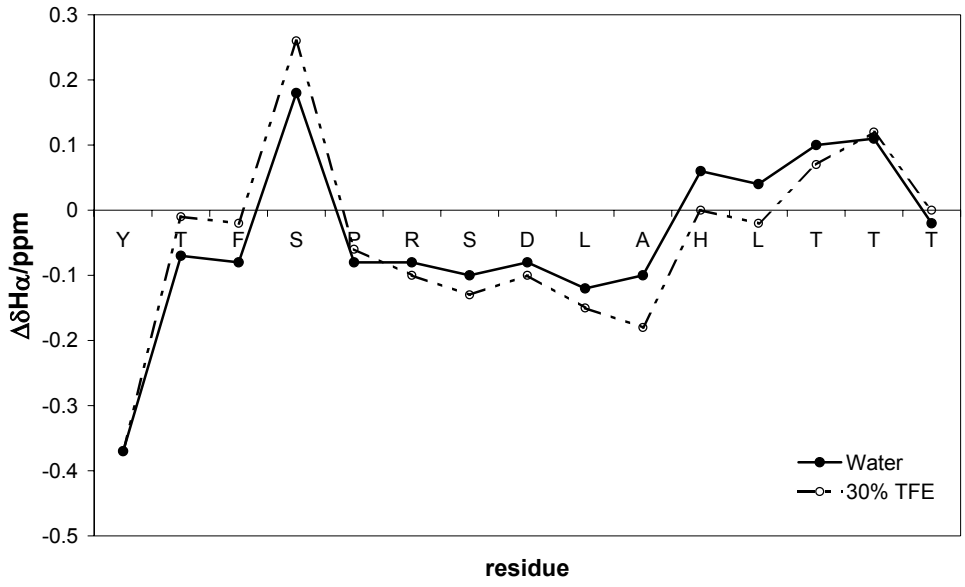

Figure 3. 17 Conformational chemical shifts observed for peptide A15(FPS) in water and 30% TFE, at 25 °C.

Conformational chemical shifts

Fig. 3.17 shows absolute conformational chemical shifts slightly higher for peptide A15(FPS) than those previously observed for the C-S30 peptides (chapter 2). The global shape of the plots resembles those observed for peptides C-S30 or C-S8c1 under identical conditions. However, the region containing the open turn at the Arg-Gly-Asp triplet and the following short helix usually observed in FMDV peptides[26,27] is longer for peptide A15(FPS). This region extends in a continuous manner from position 140 (in which an alanine is replaced by a proline) to the ^{146}His-^{147}Leu positions, including the altered Arg-***Ser***-Asp motif. The almost identical plots obtained either in water or in 30% TFE suggest that peptide A15(FPS) is not particularly sensitive to structure-inducing solvents, and thus conformationally stable.

NOEs observed

The above observations are further supported by the NOEs observed for this peptide (Fig. 3.16): despite its globally disordered structure, peptide A15(FPS) presented some interesting NOEs corresponding to $NN_{i,i+1}$ and $NN_{i,i+2}$ connectivities, located precisely in the short helical path mentioned above (Fig. 3.18). These NOEs reinforce that helical character is indeed present in the ^{142}S – ^{146}H stretch.

Compared to what was described in chapter 2 for C-S30 peptides, peptide A15(FPS) is more prone to adopt a defined structure in solution. In fact, linear peptide A15S30 did not exhibit any clearly observable NOEs in water. Only in the presence of a structuring solvent (TFE) did the C-S30 peptide exhibit NOEs similar to those observed in the case of A15(FPS). As for the more antigenic version cyc16S30, NOEs coincident to those described for A15(FPS) were observed both in water and 30% TFE. These observations further support a significant relationship between a stable peptide conformation in solution and antigenicity.

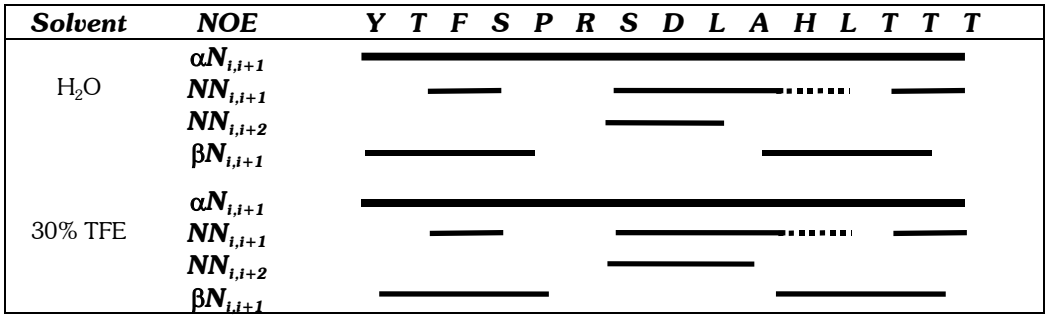

Figure 3. 18 Distribution of NOEs observed for peptide A15(FPS) in water and 30% TFE; NOE relative intensity is represented by the thickness of the bars and dotted lines correspond to possibly overlapping NOEs.

3.6 X-ray diffraction crystallography analysis of a peptide – antibody complex

3.6.0 Introduction

X-ray diffraction crystallography was employed in the structural study of the complex formed by peptide A15(138F,140P,142S) and the Fab fragment of mAb 4C4. This study was performed in collaboration with W. F. Ochoa, Dr. N. Verdaguer and Dr. I. Fita, who had been working on similar peptide – antibody complexes[1,19-21], including those between Fab 4C4 and FMDV peptides A15, A15(138F), A15(140P) and A15(142S). The present structural study had the purpose of analysing in detail eventual structural changes in the paratope – epitope interaction region, caused by the simultaneous introduction of three important mutations in the FMDV GH loop. Also, we were interested in observing how both antibody and peptide molecules managed to fit together forming a stable complex, in the presence of such amino acid replacements.

3.6.1 Determination of protein structure by X-ray crystallography[28]

Solving the three-dimensional structure of proteins by X-ray crystallography requires well-ordered and strongly X-ray diffracting crystals. However, well-ordered protein crystals are difficult to grow, due to the large size and irregular surface of protein molecules. These pack in a crystal forming large channels that occupy more than half the volume of the crystal and are filled with solvent molecules. Different protein molecules within a crystal seldom are in direct contact with each other and interactions are indirect, through several solvent layers. This feature is the reason why structures of proteins determined by X-ray crystallography are considered as the same as those for the biologically active proteins in solution. The high solvent content makes protein crystals much less resistant than their inorganic counterparts and protein crystallisation is difficult to achieve, being critically dependent on factors such as pH, temperature, protein concentration and purity, solvent, ionic strength and precipitant. Crystals are formed upon slow precipitation from supersaturated solutions. The most widely employed technique for protein crystallisation is the *hanging-drop vapour diffusion method* (Fig. 3.19), in which a droplet of protein solution (plus adequate additives) is placed on a glass cover, facing down a larger reservoir of a similar solution (with higher precipitant concentration and without protein). The droplet looses water gradually by vapour

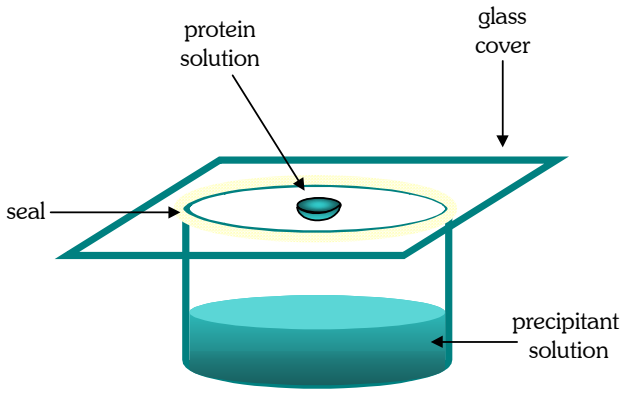

Figure 3. 19 Scheme of the hanging-drop method used in protein crystallisation (adapted from reference 30).

diffusion to the reservoir and precipitation occurs.

Crystals are submitted to X-ray diffraction analysis. X-rays are short wavelength electromagnetic radiation, resulting from electronic transitions from excited to low energy levels. Conventional X-ray sources are high-voltage tubes with a metal plate (anode) that is bombarded with accelerating electrons, X-rays of specific wavelength being emitted. *Rotating anode* X-ray generators are the most commonly found in X-ray crystallography laboratories. Much more powerful X-ray generators are *synchrotron* storage rings, in which electrons or positrons travel close to the speed of light. Strong radiation is emitted at all wavelengths, covering the X-ray spectrum. After passing through a collimator, monochromatic X-ray radiation is produced with an intensity several orders of magnitude higher than that produced by conventional X-ray sources. This allows very short exposure times in diffraction experiments and useful data can be collected from small and more sensitive crystals.

The primary beam must strike the crystal from several different directions so that all possible diffraction spots are produced. The crystal is therefore rotated during the experiment and the diffraction spots are recorded either on film or by an electronic detector. Electronic area detectors, such as the *imaging plate detector*, are a kind of electronic film where a plate covered with a photosensitive material is used to store the diffraction spots. The image thus produced is then digitised into a computer.

When a crystal is put in the path of an X-ray primary beam, some of the X-rays interact with the electrons on each crystal atom, causing them to oscillate. The oscillating electrons, in turn, emit new X-rays in all directions, a phenomenon known as *scattering*. Due to the regular three-dimensional arrangement of atoms in a crystal, the radiations emitted by the different electrons interfere with each other and, in most cases, cancel each other out. Some of them interfere positively, giving beams that are recorded as diffraction spots (Fig. 3.20).

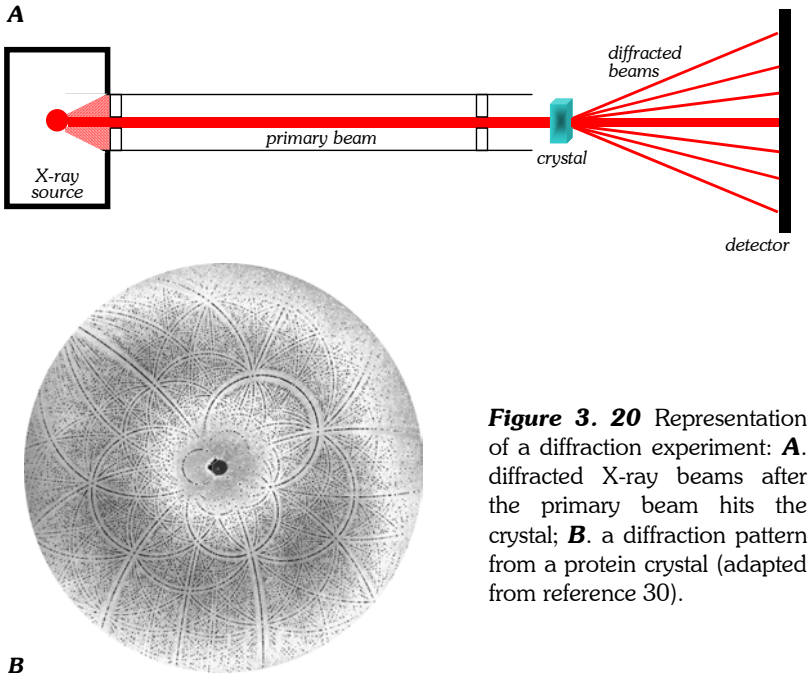

Figure 3. 20 Representation of a diffraction experiment: ***A***. diffracted X-ray beams after the primary beam hits the crystal; ***B***. a diffraction pattern from a protein crystal (adapted from reference 30).

Thus, each spot is originated by interference of all X-rays emerging from all crystal atoms with identical diffraction angle. According to Bragg's law, diffraction is regarded as reflection of the primary beam by a set of parallel planes through the unit cells of the crystal. X-rays reflected from adjacent planes travel different distances and diffraction only occurs when this difference equals the wavelength of the beam. The position of the diffraction data on the detector film relates each spot to a specific set of planes through the crystal, from which the size of the unit cell can be determined.

Each recorded spot is related to a diffracted beam characterised by its amplitude, wavelength and phase. These three parameters are needed to determine the spatial arrangement of the atoms. However, the phase is lost in X-ray diffraction experiments and this is the major problem in X-ray crystallography. The classical way to circumvent this problem in protein X-ray crystallography is based on the preparation of heavy atom protein derivatives. X-ray diffraction data from the protein alone, from the heavy atom alone and from the heavy atom protein derivative are then used to attribute initial phases to the protein atoms.
A simpler method to determine initial phases to work with is the *molecular replacement method*, which requires a known protein structure similar to the molecule under study. The phases belonging to the search model are assigned as the initial phases of the new protein structure and an electron density map is calculated.

Then, with the aid of computer graphics, a trial-and-error process is started in order to build up a model: the polypeptide main chain and side chains are matched with the electron densities and computer-aided crystallographic refinement of the model is performed. In this refinement, the model is slightly changed to minimise the differences between the experimental diffraction data and the calculated model. This difference can be given in terms of the *R factor*, a residual disagreement that is zero for total agreement and around 0.59 for total disagreement. The R factor lies between 0.15 and 0.20 for high quality data.
Non-zero R factors are seldom due to errors in the protein model. Rather, they derive from imperfections in the experimental data, such as variations in protein conformation, inaccurate solvent corrections or orientation of the micro-crystals. Therefore, the final model is an average of molecules that differ slightly both in conformation and orientation, not corresponding exactly to the real crystal.

3.6.2 General structure of immunoglobulins[28]

The basic structure of all immunoglobulins (Ig) involves two identical *heavy chains* and two identical *light chains*, linked through disulphide bonds (Fig. 3.21). The major type of immunoglobulin in human serum is the class G Ig (IgG), which is a monomer of the basic structural unit. The IgG polypeptide chain is divided into *domains* of 110 amino acid residues each; the *light chains* contain two of such domains and the *heavy chains* contain four. A light chain is composed of a *variable* amino-terminal domain (V_L) and a *constant* carboxy-terminal (C_L), whereas a heavy chain is built up from an amino-terminal variable domain (V_H) followed by three constant domains (C_{H1}, C_{H2} and C_{H3}). The variable V_L and V_H domains coincide with the *antigen binding sites* of the IgG and are not uniformly variable along their lengths: three sub-domains, called *hypervariable* or *complementarity determining regions* (CDR1, CDR2 and CDR3), show much higher variability, both in sequence and size. The CDRs are the regions that determine the specificity of the antigen – antibody interactions. Complete IgG molecules are difficult to crystallise, but their enzymatic digestion with papain or pepsin cleaves the Ig by the *hinge* region, with one *Fc* and two identical *Fab* fragments being obtained (Fig. 3.21). High resolution X-ray structural information on these fragments has shown all domains to have a similar structure, either in light or heavy chains, either in variable or constant regions. This structure is the so-called *immunoglobulin fold*, where a constant domain is formed by seven anti-parallel strands, four of which form one β sheet and the remaining three form another.

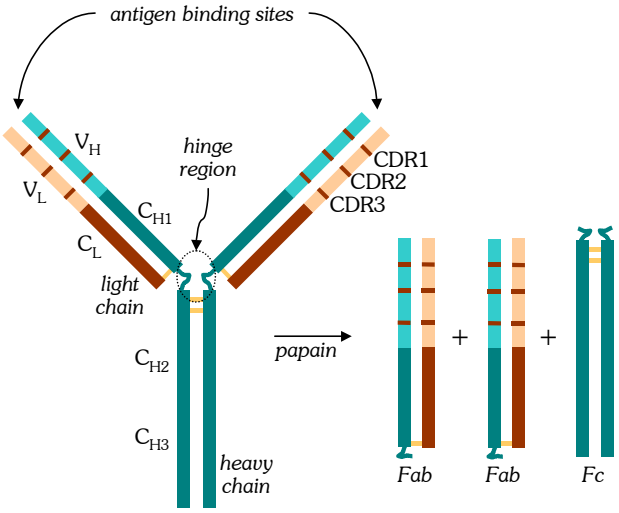

Figure 3. 21 Basic structure of an IgG and its fragments, produced by enzymatic digestion with papain (partially adapted from reference 30).

Both β sheets are closely packed together in a barrel-like arrangement (Fig. 3.22 A). The loops connecting the strands are short and thus the majority of the framework invariant residues are in the β sheets. These structural features are similar for both heavy and light chains. Variable domains are structurally similar to constant domains, but contain nine instead of seven β strands. The two additional strands are placed in the important loop region that contains the hypervariable CDR2 (Fig. 3.22 B). These extra strands provide the scaffold that renders CDR2 closer to the other two hypervariable loops CDR1 and CDR3. CDR2 and CDR3 are hairpin loops linking different strands in the five-strand β sheet, while CDR1 is a cross-over between one strand from the five-strand sheet and another from the four-strand sheet.

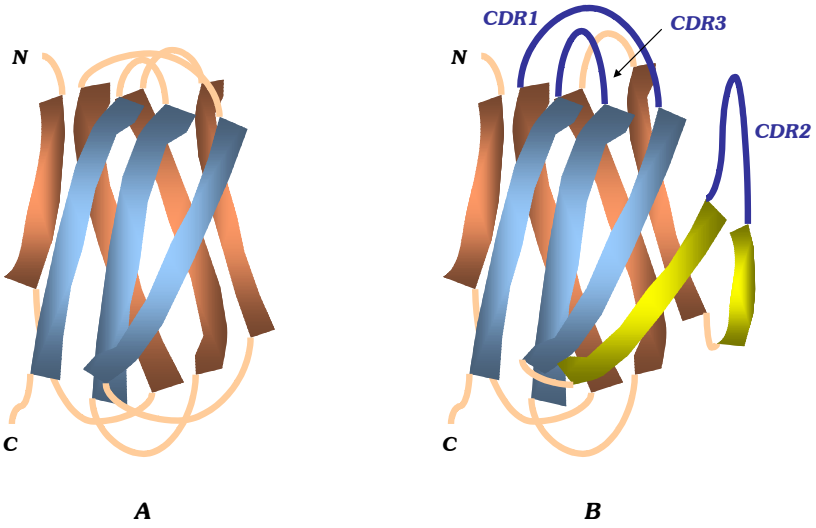

Figure 3. 22 The immunoglobulin fold: ***A***. general structure of a constant IgG domain; ***B***. general structure of a variable IgG domain (adapted from reference 30).

The Fab fragment is the "arm" of the IgG molecule that contains an intact antigen binding site. In this fragment, the heavy and light chains are tightly and extensively associated, in such a way that C_L associates with C_{H1} and V_L with V_H. Thus, a Fab fragment consists of two globular regions, one with the two constant domains and the other with the two variable domains (Fig. 3.23). While the constant domains associate by close interactions between the almost perpendicular four-strand sheets from C_H and C_L, the variable domains associate in a very different manner. In this case, the interaction area is formed by the five-strand β sheets, almost parallel to each other, and defining a barrel structure of eight (four from each five-strand sheet) antiparallel β strands. This allows the CDR loops from both variable domains to be located at the same end of the barrel, forming the complete antigen binding site.

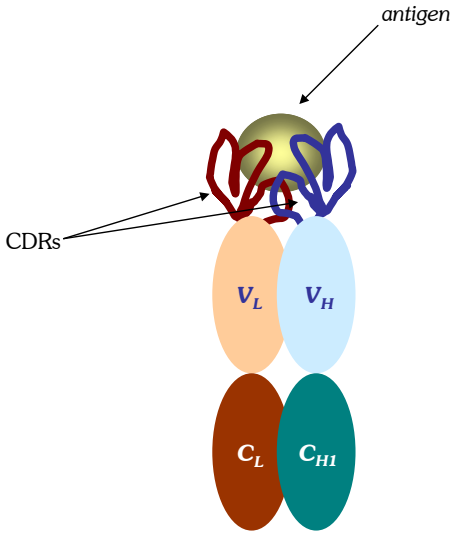

Figure 3. 23 Schematic representation of a Fab fragment: V_L/V_H and C_L/C_{H1} domains associate in such a way that CDRs can "grab" the antigen.

3.6.3 Molecular structure of the A15(FPS) – 4C4 complex in the crystal state

The protocols previously described for the crystallisation of similar FMDV peptide – Fab 4C4 complexes[20,21] proved to be readily applicable to the present case (see Materials & Methods, section 4.4.2) and crystals as those shown in Fig. 3.24 were formed. Despite the difficulties found in growing clean and perfect crystals, good diffraction data were acquired using synchrotron radiation at the European Synchrotron Radiation Facility at Grenoble, France.

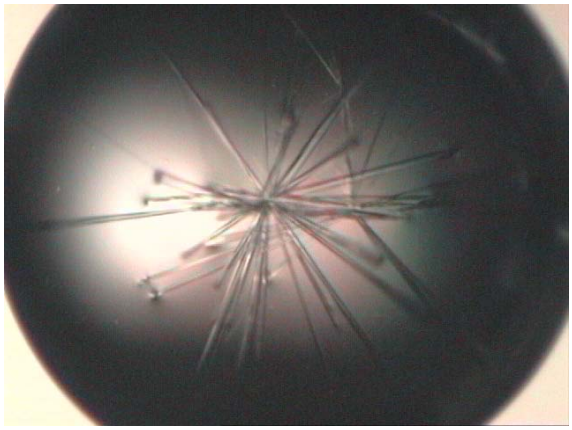

Figure 3. 24 Crystals of the A15(FPS) – 4C4 complex.

After evaluating and internally scaling the diffraction data[29] (Table 3.9), initial phases were assigned taking the known structure of Fab 4C4 as the search model[20,30]. The model was initially subjected to rigid body refinement and then treating each constant and variable domains as independent structural units. The computed electron density maps clearly showed extra density at the antigen binding site, corresponding to the peptide ligand. The peptide was then added to the model structure, which was improved by cycles of manual rebuilding with program O[31] and refinement with the CNS package[32]. The final model had an R factor of 0.22 at a 2.3 Å resolution (Table 3.9) and is represented in Fig. 3.25. The epitope – paratope contacts through hydrogen bonds are listed in Table 3.10 and matched those previously observed with the native peptide A15 in complex with the same mAb[1].

A better illustration of the present structural study requires a global appreciation of the complex, as well as of those formed between the same mAb and the three relevant single-point mutants, previously solved by W. F. Ochoa and co-workers[21]. All four peptides were shown to interact with Fab 4C4. As can be seen in Fig. 3.26, the three single-point mutants and the triple mutant all adopt a similar quasi-cyclic conformation, also shared by the native sequence A15[1,21]. This conformation seems therefore to be a key feature in the antibody – FMDV peptide recognition process. A stereoview of the A15(FPS) peptide fold in complex with Fab 4C4 is shown in Fig. 3.27.

Table 3.9 Crystallisation and diffraction data of the A15(FPS) – 4C4 complex.

Crystalisation and data collection	
Space group	***$P2_12_12_1$***
Cell parameters (Å)	***48.417***
	68.792
	145.404
Resolution (Å)	***25 – 2.2***
Overall Completeness (%)	***99.7***
R_{symm} (%)	***7.2***
Average I/σ	***10.2***
Total # of residues	
Fab	***429***
Peptide	***13***
Total # of solvent molecules	***269***
Volume solvent (%)	***48.81***
Diffraction agreement	
Resolution (Å)	***15 – 2.3***
# of reflections	***22153***
R_{free}	***0.266***
R_{factor}	***0.225***
rms deviations from ideal distance	
Bond length (Å)	***0.0179***
Bond angle (°)	***2.2193***
Average thermal factor (Å)	
Fab	***24.8***
Peptide	***24.3***
Stereochemistry of main chain	
Omega angle std. dev.	***2.0***
Bad contacts/100 res.	***0.8***
Zeta angle std. dev.	***2.0***
Stereochemistry of side chain	
Chi-1 pooled std. dev.	***11.5***

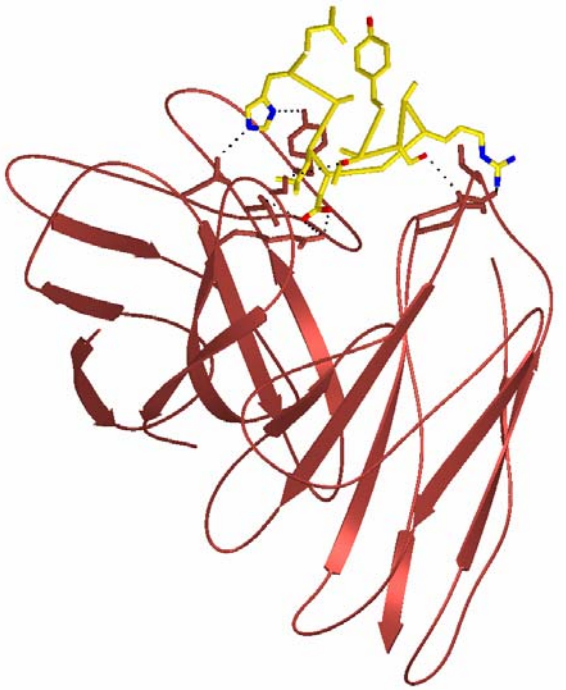

Figure 3. 25 Structure of the A15(FPS) – 4C4 complex (only Fab variable domains are shown); peptide side chains and some peptide – antibody hydrogen bonds are shown in more detail (structures built with program SETOR[33]).

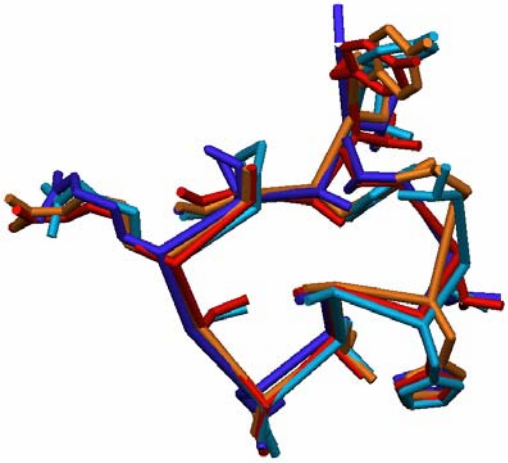

Figure 3. 26 Superposition of the structures adopted by peptides A15(138F) – red, A15(140P) – dark blue; A15(142S) – orange and A15(FPS) – light blue, when complexed with Fab 4C4 (structures built using SETOR[33]).

Table 3.10 Hydrogen bonds between antigenic peptide A15(FPS) and the Fab fragment of mAb 4C4.

Bond interaction site in		***Location***	***Distance (Å)***
Peptide	***Fab***		
Tyr136 *O*	Asn34 *Nδ2*	L1	2.6
Thr137 *O*	Asp104 *N*	H3	2.8
Thr137 *Oγ1*	Ser103 *Oγ*	H3	3.0
Ser139 *Oγ*	Asn96 *Oδ1*	L3	2.5
Arg141 *O*	Asp98 *N*	L3	2.9
Arg141 *Nη1*	Asn96 *O*	L3	3.3
Arg141 *Nη2*	Asn96 *Nδ2*	L3	3.1
Asp143 *O*	Tyr59 *Oη*	H2	3.8
Asp143 *Oδ1*	Thr50 *Oγ1*	H2	2.7
Asp143 *Oδ1*	Arg99 *Nε*	H3	2.7
Asp143 *Oδ2*	Arg99 *Nη2*	H3	2.7
His146 *Nδ1*	Tyr59 *Oη*	H2	2.9
His146 *Nδ2*	Thr33 *Oγ1*	H1	3.0

Note: letters L and H in the *location* column stand for light and heavy chain, respectively, and are followed by numbers indicating the CDR where the antibody residue is located.

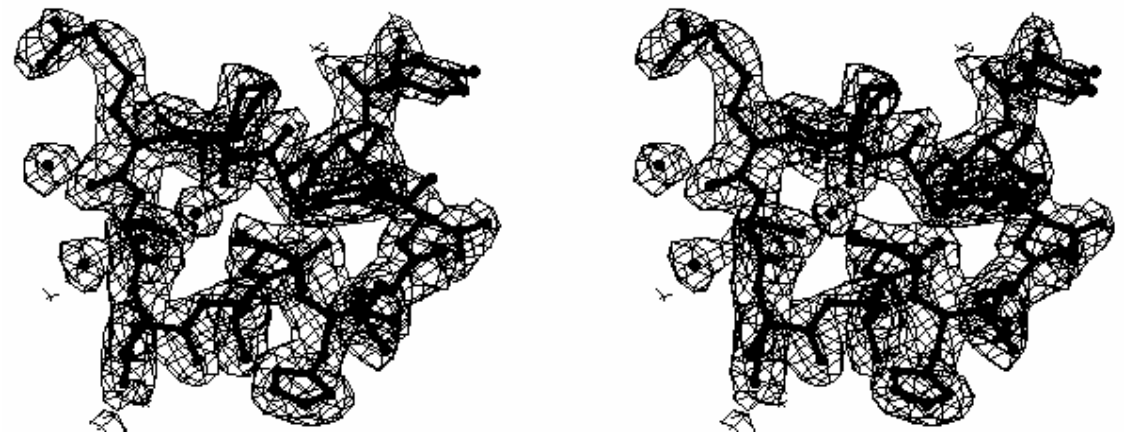

Figure 3. 27 Stereoview of the Fo-Fc omit map of peptide A15(FPS) at 2.3 Å resolution; the peptide final model, including water molecules, was also shown for clarity; residues 149 and 150 were not considered in the model (image generated with program SETOR[33]).

The similarity found in both peptide folding and epitope – paratope interactions for all FMDV peptide – antibody complexes studied so far is remarkable. In view of this, we can devise the following requirements for the recognition of FMDV peptides by anti-site A mAbs:

Fab-peptide interactions

Important interactions between peptide residues and the Fab cannot be bypassed, which is confirmed by the absence of Fab-recognition of peptide mutants where key residues had been replaced[1,34,35]. These interactions mainly involve peptide residues 141, 143 and 146 (Table 3.10). They are similar to several other resolved structures[1,20,21] and strong hydrogen bonds are seen to stabilise the complex scaffold. Other observed interactions, particular to each complex, can explain affinity differences between the different complexes, but do not seem to be absolutely necessary.

Peptide conformation

The hydrogen bonds between peptide residues and Fab do not seem to be sufficient to ensure a strong interaction, since a precise peptide conformation seems to be an important requirement for peptide-Fab union. Such conformation involves two important features:

Hydrophobic cavity

In all peptides studied a hydrophobic cavity was observed[1,18-21], mainly formed by residues 138, 144 and 147. These residues engage in strong hydrophobic interactions through their side chains, stabilising peptide conformation. Mutations at these positions would imply the loss of such cavity and, therefore, a decrease in the stability of the peptide-Fab complex. However, that does not occur with the ^{138}Ala→Phe replacement; in this case, the Phe side chain is oriented into the cavity, and not only does not disrupt hydrophobic interactions, but in fact stabilises the cavity itself (Fig. 3.26, 3.27).

Intrapeptide interactions

There is a set of interactions between the different peptide residues which contribute to peptide folding, such as hydrogen bonds between the different nitrogen and oxygen atoms of the main chain and also the presence of several water molecules bridge-bonding peptide residues. These are key interactions that restrict mutations to those amino acids able to preserve this type of structural arrangement. A remarkable example is the ^{142}Gly→Ser mutation, in which the side chain hydroxyl group of Ser replaces a water molecule present in the structures where ^{142}Gly is conserved (Fig. 3.28), maintaining the turn characteristic of the RXD motif (X=Gly or Ser). Pro at position 140 also helps in the stabilisation of such a turn.

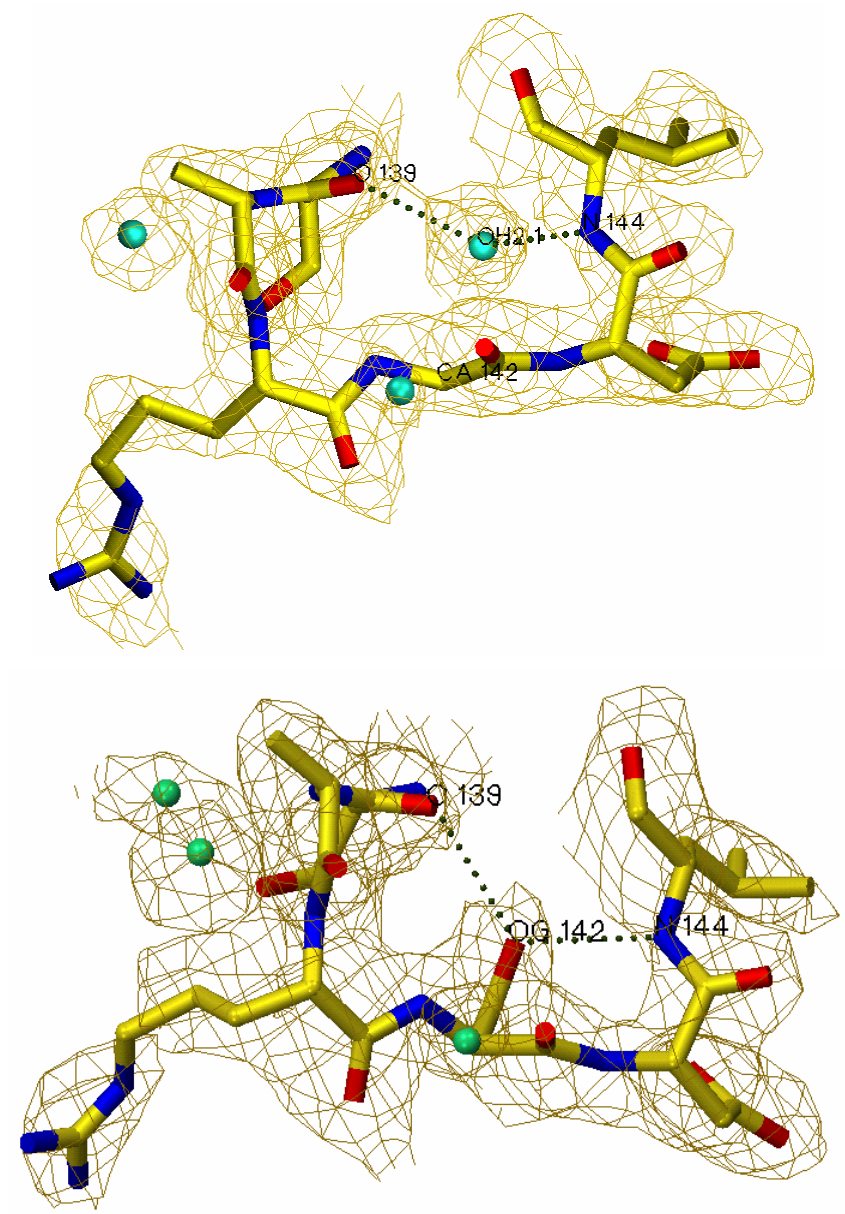

Figure 3. 28 Detailed view of the RXD turn, with X=Gly and X=Ser for the upper [peptide A15(138F)] and lower [peptide A15(142S)] structures, respectively; the corresponding Fo-Fc omit maps are also shown. As it can be seen, the RGD turn is held up by hydrogen bridging between Ser139 O – H_2O – Leu144 N (above), while the RSD turn is stabilised by similar hydrogen bridging between Ser139 O – Ser142 Oγ – Leu144 N (below). Structures were built with SETOR[33].

3.7 Recapitulation

This chapter was focused on the study of 15-residue peptides from the GH loop of FMDV. The peptide sequences were based on the reference FMDV strain C-S8c1, bearing combinations of the replacements $^{137}T \rightarrow I$, $^{138}A \rightarrow F$, $^{140}A \rightarrow P$, $^{142}G \rightarrow S$ and $^{148}T \rightarrow I$. These amino acid replacements were interesting in the sense that the corresponding single-point mutants had been previously found to be significantly antigenic towards several anti-GH loop neutralising mAbs[1]. Therefore, the question was raised whether multiple combination of these replacements could lead to positive synergistic effects, yielding promising peptide antigens. Also, three such replacements deserved further attention: position 138 was known to play a role in intrapeptide interactions[1,20] and the much larger size of the Phe side chain seemed unlikely to be "ignored" by antibodies; the introduction of a Pro in the loop, with its peculiar structural behaviour, deserved to be analysed; and the effect of replacing Gly by Ser in the highly conserved, key RGD motif, also captured our attention.

These peptides were fully characterised as FMDV antigens by means of SPR studies, towards three anti-site A mAbs. It was immediately observed that this peptide family was quite different from the one discussed in chapter 2. In fact, all these peptides displayed high antigenicities, which prevented the kinetic study of their interactions with the mAbs due to mass-transport limitations. High association rate constants, very slow dissociations and/or incomplete surface regeneration were persistently observed and alternative solution affinity SPR analyses were performed. These confirmed the high peptide – antibody affinities expected, generally comparable to or even higher than those displayed by the native sequence represented by peptide A15.

The fact that these multiple mutants were fully recognised by anti-site A neutralising mAbs was quite interesting and led to other questions, such as *how did the mutations affect peptide conformation* and *how did the antibody paratope adapt to these mutations*. We approached the first question through a two-dimensional ^{1}H-NMR study of peptide A15(FPS) in solution and the second one by means of an X-ray diffraction crystallography study of the complex formed between mAb 4C4 and the same peptide. The NMR characterisation of peptide A15(FPS) in solution showed that this peptide had a conformational behaviour quite similar to that previously observed for the native sequence A15[26,27]. Data suggested an open turn in the RSD region followed by an incipient short α-helix up to residue 147, features which had been previously recognised in peptide A15 and regarded as antigenically relevant[26,27,34].

The diffraction study of the A15(FPS) – 4C4 complex showed that the pattern of antibody – antigen interactions is identical for all FMDV peptides studied so far[1,18-21]. Thus, a stable mAb – peptide complex can be formed as long as some key requisites are fulfilled. These involve specific residues committed in direct epitope – paratope contacts (^{141}Arg, ^{143}Asp, ^{146}His) and residues able to stabilise a particular peptide conformation. This conformation corresponds to a quasi-cyclic folding around a hydrophobic cavity defined by residues 138, 144 and 147 and to other important intrapeptide hydrogen bonds defining the central open turn involving positions 141, 142 and 143. Amino acid replacements that not only do not disrupt, but even help to promote these essential requirements for mAb recognition can yield peptides with significant reactivity towards anti-FMDV neutralising mAbs and thus useful as FMDV antigens.

References

1 Verdaguer, N., Sevilla, N., Valero, M. L., Stuart, D., Brocchi, E., Andreu, D., Giralt, E., Domingo, E., Mateu, M. G. and Fita, I. (1998) A similar pattern of interaction for different antibodies with a major antigenic site of foot-and-mouth disease virus: implications for intratypic antigenic variation, *J. Virol.* ***72***, 739-748.

2 Valero, M. L. "Mimetización estructural e inmunogénica del sitio antigénico principal del virus de la fiebre aftosa" (Ph. D. Thesis), Department of Organic Chemistry – University of Barcelona: 1997.

3 Mateu, M. G., Valero, M. L., Andreu, D. and Domingo, E. (1996) Systematic replacement of amino acid residues within an Arg-Gly-Asp containing loop of foot-and-mouth disease virus and effect on cell recognition, *J. Biol. Chem.* ***271***, 12814-12819.

4 O'Shannessy, D. J. and Winzor, D. J. (1996) Interpretation of deviations from pseudo-first-order kinetic behavior in the characterization of ligand binding by biosensor technology, *Anal. Biochem.* ***236***, 275-283.

5 Schuck, P. (1997) Reliable determination of binding affinity and kinetics using surface plasmon resonance biosensors, *Curr. Op. Biotech.* ***8***, 498-502.

6 Hall, D. R., Cann, J. R. and Winzor, D. J. (1996) Demonstration of an upper limit to the range of association rate constants amenable to study by biosensor technology based on surface plasmon resonance, *Anal. Biochem.* ***235***, 175-184.

7 Karlsson, R. (1994) Real-time competitive kinetic analysis of interactions between low-molecular-weight ligands in solution and surface-immobilized receptors, *Anal. Biochem.* ***221***, 142-151.

8 Albericio, F., Andreu, D., Giralt, E., Navalpotro, C., Pedroso, E., Ponsati, B. and Ruiz-Gayo, M. (1989) Use of the Npys thiol protection in solid phase peptide synthesis, *Int. J. Peptide Protein Res.* ***34***, 124-128.

9 Benito, A., Mateu, M. G. and Villaverde, A. (1995) Improved mimicry of a foot-and-mouth disease virus antigenic site by a viral peptide displayed on β-galactosidase surface, *Biotechnology* ***13***, 801-804.

10 Carbonell, X., Benito, A. and Villaverde, A. (1996) Converging antigenic structure of a recombinant viral peptide displayed on different frameworks of carrier proteins, *FEBS Lett.* ***397***, 169-172.

11 Feliu, J. X., Benito, A., Oliva, B., Avilés, F. X. and Villaverde, A. (1998) Conformational flexibility in a highly mobile protein loop of foot-and-mouth disease virus: distinct structural requirements for integrin and antibody binding, *J. Mol. Biol.* ***283***, 331-338.

12 Feliu, J. X. and Villaverde, A. (1998) Engineering of solvent-exposed loops in Escherichia coli β-galactosidase, *FEBS Lett.* ***434***, 23-27.

13 Andersson, K., Hamalainen, M. and Malmqvist, M. (1999) Identification and optimization of regeneration conditions for affinity-based biosensor assays. A multivariate cocktail approach, *Anal. Chem.* ***71***, 2475-2481.

14 Lapko, V. N., Jiang, X. Y. and Smith, D. L. (1998) Surface topography of phytocrome A deduced from specific chemical modification with iodoacetamide, Biochemistry ***37***, 12526-12535.

15 Nieba, L., Krebber, A. and Plükthun, A. (1996) Competition BIAcore for measuring true affinities: large differences from values determined from binding kinetics, *Anal. Biochem.* ***234***, 155-165.

16 "BIAapplications Handbook", (Pharmacia Biosensor AB, 1994) Uppsala, Sweden.

17 Lazareno, S. and Birdsall, N. J. (1993) Estimation of competitive antagonist affinity from functional inhibition curves using the Gaddum, Schild and Cheng-Prusoff equations, *British J. Pharmacol.* ***109***, 1110-1119.

18 Verdaguer, N., Mateu, M. G., Andreu, D., Giralt, E., Domingo, E. and Fita, I. (1995) Structure of the major antigenic loop of foot-and-mouth disease virus complexed with a neutralizing antibody: direct involvment of the Arg-Gly-Asp motif in the interaction, *EMBO J.* ***14***, 1690-1696.

19 Verdaguer, N., Mateu, M. G., Bravo, J., Domingo, E. and Fita, I. (1996) Induced pocket to accomodate the cell attachment site Arg-Gly-Asp motif in a neutralizing antibody against foot-and-mouth disease virus, *J. Mol. Biol*. ***256***, 364-376.

20 Ochoa, W. F., Kalko, S., Mateu, M., Gomes, P., Andreu, D., Domingo, E., Fita, I. and Verdaguer, N. (2000) A multiply substituted GH loop from foot-and-mouth disease virus in complex with a neutralizing antibody: a role for water molecules, *J. Gen. Virol.* ***81***, 1495-1505.

21 Ochoa, W. F. *et al.*, manuscript in preparation.

22 Wüthrich, K. "NMR of proteins and nucleic acids", Wiley, New York (1986).

23 Braunschweiler, L. and Ernst, R. R. (1983), *J. Magn. Reson.* ***53***, 521.

24 Kumar, A., Ernst, R. R. and Wüthrich, K. (1980), *Biochem. Biophys. Chem. Comm.* ***95***, 1.

25 Bothner-By, A. A., Stephens, R. L., Lee, J., Warren, C. D. and Jeanloz, R. W. (1984) Structure determination of a tetrasaccharide: transient nuclear overhauser effects in the rotating frame, *J. Am. Chem. Soc.* ***106***, 811-813.

26 Haack, T., Camarero, J. A., Roig, X., Mateu, M. G., Domingo, E., Andreu, D. and Giralt, E. (1997) A cyclic disulfide peptide reproduces in solution the main structural features of a native antigenic site of foot-and-mouth disease virus, *Int. J. Biol. Macromol.* ***20***, 209-219.

27 Valero, M. L., Camarero, J. A., Haack, T., Mateu, M. G., Domingo, E., Giralt, E. and Andreu, D. (2000) Native-like cyclic peptide models of a viral antigenic site: finding a balance between rigidity and flexibility, *J. Mol. Recognit.* ***13***, 5-13.

28 Branden, C. and Tooze, J., "Introduction to protein structure", Garland Publishing Inc., New York (1991).

29 Otwinowsky, Z. and Minor, W. (1997) Processing of X-ray diffraction data collected in oscillation mode, *Methods Enzymol.* ***276***, 307-326.

30 Rossman, M. G. (Ed.) "The molecular replacement method", Gordon & Breach, New York (1972).

31 Jones, T. A., Zou, J. Y., Cowan, S. W. and Kjeldgaard, M. (1991) Improved methods for building protein models in electron density maps and the location of errors in these models, *Acta Crystallogr. A* ***47***, 110-119.

32 Brünger, A. T., Adams, P. D., Clore, G. M., DeLano, W. L., Gros, P., Grosse-Kunstleve, R. W., Jiang, J.-S., Kuszewski, J., Nilges, M., Pannu, N. S., Read, R. J., Rice, L. M., Simonson, T. and Warren, G. L. (1998) *Acta Crystallogr. D* ***54***, 905-921.

33 Evans, S. V. (1993) SETOR: hardware-lighted three-dimensional solid model representations of macromolecules, *J. Molec. Graphics* ***11***, 134-138.

34 Mateu, M. G. (1995) Antibody recognition of picornaviruses and escape from neutralisation: a structural view, *Virus Res.* ***38***, 1-24.

35 Domingo, E., Verdaguer, N., Ochoa, W. F., Ruiz-Jarabo, C. M., Sevilla, N., Baranowski, E., Mateu, M. G. and Fita, I. (1999) Biochemical and structural studies with neutralising antibodies raised against foot-and-mouth disease virus, *Virus Res.* ***62***, 169-175.